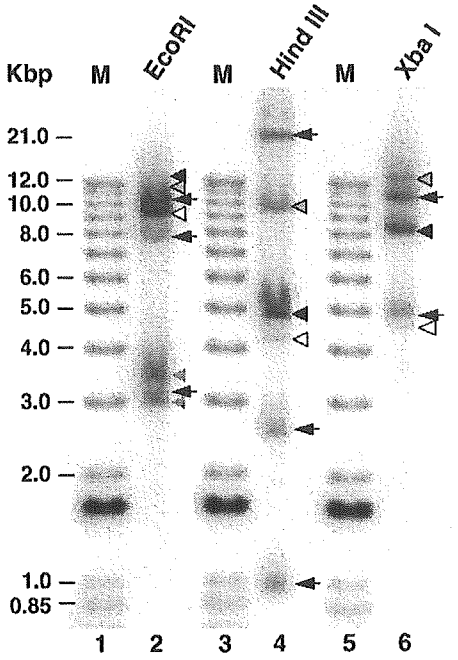

Figure 6. Southern blot analyses of genomic DNA for mouse *Itpa*-related sequences. Genomic DNA (10 μg) prepared from CCE ES cells was digested with *Eco*RI (lane 2), *Hind*III (lane 4) or *Xba*I (lane 6), and was subjected to Southern blot analyses with ^{32}P-labeled fragment containing the entire coding region from the type A *Itpa* cDNA (731 bp). Southern hybridization was done as previously described,[27] and the membrane was washed twice in 2× SSC/0.1% SDS, and then once in 0.2×SSC/0.1% SDS. The arrows indicate bands corresponding to the expected fragments from *Itpa* gene, closed arrowheads indicate bands corresponding to the expected fragments from pseudogene α, the gray arrowheads with solid line indicates the bands corresponding to the expected fragments from pseudogene β, while the gray arrowheads without solid line indicate band(s) whose size could not be predicted precisely because of incompleteness of the database. The open arrowheads indicate bands corresponding to the expected fragments from pseudogene γ (Table 2).

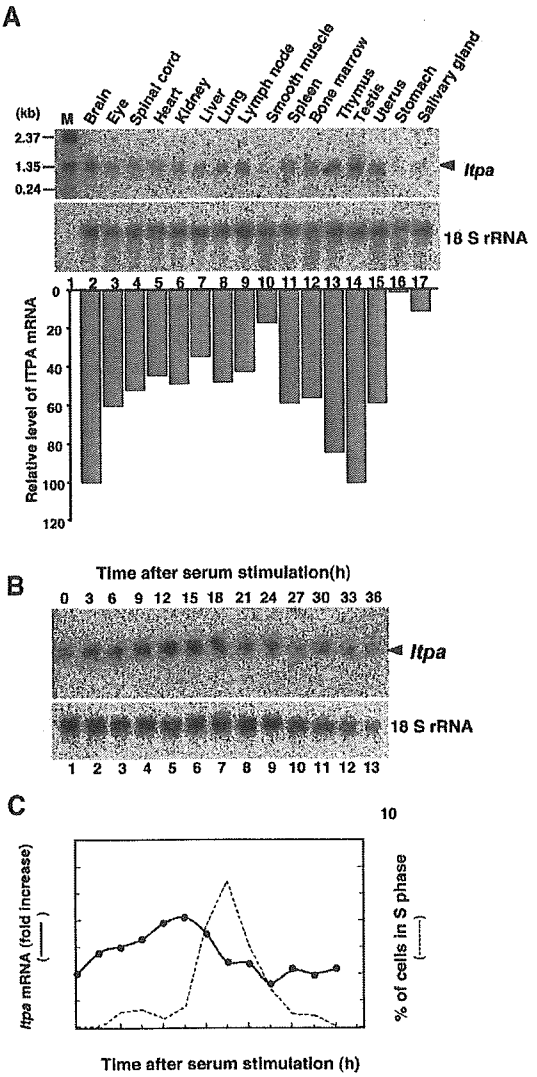

Figure 7. Expression of mouse *Itpa* gene in mouse tissue and its association with cell proliferation. *A*. The expression of *Itpa* mRNA in various types of adult mouse tissue. Total RNAs (20 μg each) extracted from various types of mouse tissue were electrophoresed, transferred onto a Hybond^{TM}-N^{+} nylon membrane, and subsequently probed with ^{32}P-labeled fragment containing the entire coding region from the type A *Itpa* cDNA (731 bp) (top panel) and the 18S rRNA probe[49] (middle panel), as previously described.[50] The arrowhead indicates *Itpa* mRNA. In the bottom panel, the relative amounts of *Itpa* mRNA to *18S rRNA* were calculated based on the radioactivity. The ratio of the relative amount of each transcript to that in the testis is shown. *B*. The expression of *Itpa* mRNA in quiescent and serum-stimulated BALB/c3T3 cells. The total RNA isolated was subjected to Northern blot analyses to determine the expression amount of *Itpa* mRNA and 18S rRNA. *C*. The relative amounts of *Itpa* mRNA to 18S rRNA were calculated based on radioactivity. The ratio of the relative amount of each transcript to that in the quiescent cells is shown (closed circle). The percentages of the cells in the S phase of the cell cycle were determined by flow cytometry as previously described[28] and then were plotted with a dotted line.

TATA-less promoter with a sequence (CTACTTC) which exactly matched the consensus sequence for the initiator (PyPyANT/APyPy), just upstream of the 5′ end of the longest *Itpa* cDNA (Fig. 5B),[34] indicating that the *Itpa* gene is likely to be one of the housekeeping genes which are ubiquitously expressed. A consensus-like sequence for ELK1 or ETS-1 proteins (ACMGGAAGTNC, ACMGGAWRTT), which are known to be activated during serum stimulation,[35,36] and one for GATA transcription factors (WGATAR)[37] were found in the *Itpa* promoter region (Fig. 5B). Those factors may be responsible for the inducible expression of *Itpa* in some tissues.

3.6. Expression and distribution of mouse ITPA protein in mouse tissue

In extract prepared from mouse brain, only a single band corresponding to a polypeptide with a molecular

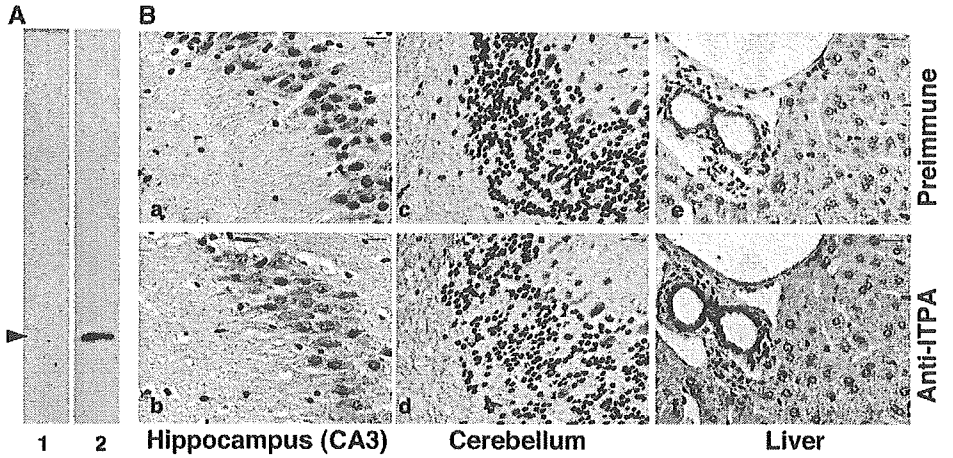

Figure 8. The expression of mouse ITPA protein in mouse tissues. *A*. Western blotting analysis. Brain extracts (20 μg protein) were separated on 12.5% SDS-PAGE and subjected to Western blotting as previously described,[31] with preimmune serum (lane 1) or anti-ITPA serum (lane 2). The arrowhead indicates the 22-kDa polypeptide. *B*. Immunohistochemistry. Brain (panels a–d) and liver (panels e, f) sections embedded in paraffin blocks were subjected to immunohistochemical analyses with the anti-ITPA serum (panels b, d, f) and preimmune serum (panels a, c, e) as controls. The nuclei were counterstained with hematoxylin (blue).

weight of 22 kDa was reacted with the anti-ITPA serum but not with preimmune serum (Fig. 8A), thus indicating that the anti-ITPA serum specifically reacts with mouse ITPA in the extract. We could not detect smaller polypeptides in either cellular or tissue extracts reacted with the anti-ITPA serum; therefore, it remains to be established as to whether type B or C *Itpa* transcripts produce any polypeptide *in vivo*.

Next, brain and liver sections embedded in paraffin blocks were subjected to immunohistochemistry using the anti-ITPA and preimmune sera as controls (Fig. 8B). In the brain, the anti-ITPA serum exhibited apparent immunoreactivity throughout the brain section in comparison to the preimmune serum (data not shown). In the brain section, most of the hippocampal neurons in CA1 to CA3 and DG exhibited relatively strong ITPA immunoreactivity, especially in the soma of CA3 pyramidal cells and mossy fibers (Fig. 8Ba, b). In the cerebellum, the cell bodies of Purkinje cells and mossy fibers in the cerebellar white matter exhibited a strong ITPA immunoreactivity, while granule cell bodies exhibited a relatively weak immunoreactivity (Fig. 8c, d). In the liver, hepatocytes exhibited an evenly distributed ITPA immunoreactivity mainly in the cytoplasm, and a significantly strong immunoreactivity was seen in the cytoplasm and nuclei of the epithelial cells lined bile ducts, and to a lesser extent those of the endothelial cells lined the portal vein (Fig. 8Be, f).

The expression profile of *Itpa* suggests that the ITPA function may be required for proliferative tissues as well as postmitotic neurons. In neurons, ITPA protein was mostly detected in the cytoplasm, to a lesser extent in the nucleus and also in nerve fibers. A particularly high level of expression was apparent in hippocampal CA3 pyramidal cells and Purkinje cells in the cerebellum. Those neurons were postmitotic, thus suggesting that ITPA may function to sanitize the nucleotide pools for RNA synthesis or DNA synthesis in the mitochondria. However, the PSORT II program (http://psort.nibb.ac.jp/) to predict the protein localization sites in cells,[38] predicted that human and mouse ITPA proteins are likely to mostly localize in the cytoplasm and some in the nucleus but not in the mitochondria, and thus ITPA may not function in mitochondria.

On the other hand, the localization of ITPA in nerve fibers may indicate that ITP/dITP or XTP/dXTP, substrate nucleotides for ITPA, may be toxic for the neural function when such abnormal nucleotides accumulated in the nerve fibers. It is well known that nitric oxide (NO), a neurotransmitter,[39] promotes the deamination of various molecules such as nucleic acids and proteins,[40–42] thus increasing the intracellular concentration of ITP/dITP or XTP/dXTP which can be generated by the deamination of ATP/dATP or GTP/dGTP.[20] It has recently been shown that ITP or XTP disturbs the small G protein function through competition with GTP,[43–45] thus suggesting that the hydrolysis of ITP/XTP by ITPA is critical for maintaining such signal transduction through small G proteins, especially in neurons. As a result, ITPA may protect the neurons from damage caused by these abnormal nucleotides.

In the liver, a much higher level of ITPA was detected in the epithelial cell-lined bile duct and also in the endothelial cell-lined portal vein than in hepatocytes. In the endothelial cells, again NO plays an important role in regulating vasoconstriction, thus a high level of ITPA may be required.[46] In the bile duct, a high level of ITPA was detected in the nuclei of epithelial cells, suggesting that those cells have greater exposure to deamination by chemicals excreted through the bile duct as well as

NO.[47,48]

In conclusion, among various genomic sequences highly homologous to human ITPA coding sequences in the mouse, the mouse ortholog (*mItpa*) for hITPA was successfully isolated by the retro-recombination method, while a processed-*Itpa* gene like sequence and two pseudogenes were also identified in the mouse genome. Since no transcribed sequence derived from the processed *Itpa*-like sequence was found in any of the examined mouse tissue specimens, we thus conclude that the mouse has only one functional *Itpa* gene, which is highly expressed in the testis, brain and thymus.

Acknowledgements: We thank Dr. Daniel Nathans for BALB/c 3T3 cells, Dr. Motoya Katsuki for CCE ES cells, Drs. Masato Furuichi and Yoshimichi Nakatsu for their helpful discussions, Setsuko Kitamura and Keiko Aiura for their technical assistance, Dr. B. Quinn for comments on the manuscript. This work was supported by grants from CREST, Japan Science and Technology Agency, the Ministry of Education, Culture, Sports, Science, and Technology of Japan (grant number: 16012248), and the Japan Society for the Promotion of Science (grant numbers: 15590347, 16390119).

References

1. Nakabeppu, Y., Tsuchimoto, D., Furuichi, M., and Sakumi, K. 2004, The Defense Mechanisms in Mammalian Cells Against Oxidative Damage in Nucleic Acids and Their Involvement in the Suppression of Mutagenesis and Cell Death, *Free Radic. Res.*, **38**, 423–429.
2. Kamiya, H. and Kasai, H. 1995, Formation of 2-hydroxydeoxyadenosine triphosphate, an oxidatively damaged nucleotide, and its incorporation by DNA polymerases. Steady-state kinetics of the incorporation, *J. Biol. Chem.*, **270**, 19446–19450.
3. Sekiguchi, M. 1996, MutT-related error avoidance mechanism for DNA synthesis, *Genes Cells*, **1**, 139–145.
4. Tye, B. K., Nyman, P. O., Lehman, I. R., Hochhauser, S., and Weiss, B. 1977, Transient accumulation of Okazaki fragments as a result of uracil incorporation into nascent DNA, *Proc. Natl. Acad. Sci. U.S.A.*, **74**, 154–157.
5. Hochhauser, S. J. and Weiss, B. 1978, *Escherichia coli* mutants deficient in deoxyuridine triphosphatase, *J. Bacteriol.*, **134**, 157–166.
6. Gadsden, M. H., McIntosh, E. M., Game, J. C., Wilson, P. J., and Haynes, R. H. 1993, dUTP pyrophosphatase is an essential enzyme in *Saccharomyces cerevisiae*, *Embo J.*, **12**, 4425–4431.
7. Kouzminova, E. A. and Kuzminov, A. 2004, Chromosomal fragmentation in dUTPase-deficient mutants of *Escherichia coli* and its recombinational repair, *Mol. Microbiol.*, **51**, 1279–1295.
8. Maki, H. and Sekiguchi, M. 1992, MutT protein specifically hydrolyses a potent mutagenic substrate for DNA synthesis, *Nature*, **355**, 273–275.
9. Fujii, Y., Shimokawa, H., Sekiguchi, M., and Nakabeppu, Y. 1999, Functional significance of the conserved residues for the 23-residue module among MTH1 and MutT family proteins, *J. Biol. Chem.*, **274**, 38251–38259.
10. Tsuzuki, T., Egashira, A., Igarashi, H. et al. 2001, Spontaneous tumorigenesis in mice defective in the *MTH1* gene encoding 8-oxo-dGTPase, *Proc. Natl. Acad. Sci. U.S.A.*, **98**, 11456–11461.
11. Nakabeppu, Y. 2001, Molecular genetics and structural biology of human MutT homolog, MTH1, *Mutat. Res.*, **477**, 59–70.
12. Sakai, Y., Furuichi, M., Takahashi, M. et al. 2002, A molecular basis for the selective recognition of 2-hydroxy-dATP and 8-Oxo-dGTP by human MTH1, *J. Biol. Chem.*, **277**, 8579–8587.
13. Bessman, M. J., Frick, D. N., and O'Handley, S. F. 1996, The MutT proteins or "Nudix" hydrolases, a family of versatile, widely distributed, "housecleaning" enzymes, *J. Biol. Chem.*, **271**, 25059–25062.
14. Ishibashi, T., Hayakawa, H., and Sekiguchi, M. 2003, A novel mechanism for preventing mutations caused by oxidation of guanine nucleotides, *EMBO Rep.*, **4**, 479–483.
15. Cai, J. P., Ishibashi, T., Takagi, Y., Hayakawa, H., and Sekiguchi, M. 2003, Mouse MTH2 protein which prevents mutations caused by 8-oxoguanine nucleotides. Biochem, *Biophys. Res. Commun.*, **305**, 1073–1077.
16. Kamiya, H., Iida, E., and Harashima, H. 2004, Important amino acids in the phosphohydrolase module of *Escherichia coli* Orf135, *Biochem. Biophys. Res. Commun.*, **323**, 1063–1068.
17. Nunoshiba, T., Ishida, R., Sasaki, S., Iwai, S., Nakabeppu, Y., and Yamamoto, K. 2004, A novel Nudix hydrolase for oxidized purine nucleoside triphosphates encoded by *ORFYLR151c* (*PCD1* gene) in *Saccharomyces cerevisiae*, *Nucleic Acids Res.*, **32**, 5339–5348.
18. Hwang, K. Y., Chung, J. H., Kim, S. H., Han, Y. S., and Cho, Y. 1999, Structure-based identification of a novel NTPase from *Methanococcus jannaschii*, *Nat. Struct. Biol.*, **6**, 691–696.
19. Lin, S., McLennan, A. G., Ying, K. et al. 2001, Cloning, expression, and characterization of a human inosine triphosphate pyrophosphatase encoded by the *ITPA* gene, *J. Biol. Chem.*, **276**, 18695–18701.
20. Chung, J. H., Park, H. Y., Lee, J. H., and Jang, Y. 2002, Identification of the dITP- and XTP-hydrolyzing protein from *Escherichia coli*, *J. Biochem. Mol. Biol.*, **35**, 403–408.
21. Clyman, J. and Cunningham, R. P. 1987, *Escherichia coli* K-12 mutants in which viability is dependent on recA function, *J. Bacteriol.*, **169**, 4203–4210.
22. Bradshaw, J. S. and Kuzminov, A. 2003, RdgB acts to avoid chromosome fragmentation in *Escherichia coli*, *Mol. Microbiol.*, **48**, 1711–1725.
23. Vanderheiden, B. S. 1964, Inosine triphosphate in human erythrocytes: a genetic treat. *Proc. Xth. Congress Int. Soc. Blood. Transf., Stockholm*, pp. 540–548.
24. Cao, H. and Hegele, R. A. 2002, DNA polymorphisms in *ITPA* including basis of inosine triphosphatase deficiency, *J. Hum. Genet.*, **47**, 620–622.
25. Sumi, S., Marinaki, A. M., Arenas, M. et al. 2002, Genetic basis of inosine triphosphate pyrophosphohydrolase deficiency, *Hum. Genet.*, **111**, 360–367.
26. Hirano, S., Tominaga, Y., Ichinoe, A. et al. 2003, Muta-

tor Phenotype of MUTYH-null Mouse Embryonic Stem Cells, *J. Biol. Chem.*, **278**, 38121–38124.
27. Ide, Y., Tsuchimoto, D., Tominaga, Y., Iwamoto, Y., and Nakabeppu, Y. 2003, Characterization of the genomic structure and expression of the mouse *Apex2* gene, *Genomics*, **81**, 47–57.
28. Nakabeppu, Y., Oda, S., and Sekiguchi, M. 1993, Proliferative activation of quiescent Rat-1A cells by ΔFosB, *Mol. Cell. Biol.*, **13**, 4157–4166.
29. Woltjen, K., Bain, G., and Rancourt, D. E. 2000, Retrorecombination screening of a mouse embryonic stem cell genomic library, *Nucleic Acids Res.*, **28**, E41.
30. Nakabeppu, Y. and Nathans, D. 1991, A naturally occurring truncated form of FosB that inhibits Fos/Jun transcriptional activity, *Cell*, **64**, 751–759.
31. Tsuchimoto, D., Sakai, Y., Sakumi, K. et al. 2001, Human APE2 protein is mostly localized in the nuclei and to some extent in the mitochondria, while nuclear APE2 is partly associated with proliferating cell nuclear antigen, *Nucleic Acids Res.*, **29**, 2349–2360.
32. Burset, M., Seledtsov, I. A., and Solovyev, V. V. 2000, Analysis of canonical and non-canonical splice sites in mammalian genomes, *Nucleic Acids Res.*, **28**, 4364–4375.
33. Burset, M., Seledtsov, I. A., and Solovyev, V. V. 2001, SpliceDB: database of canonical and non-canonical mammalian splice sites, *Nucleic Acids Res.*, **29**, 255–259.
34. Butler, J. E. and Kadonaga, J. T. 2002, The RNA polymerase II core promoter: a key component in the regulation of gene expression, *Genes Dev.*, **16**, 2583–2592.
35. Rao, V. N. and Reddy, E. S. 1992, A divergent ets-related protein, elk-1, recognizes similar c-ets-1 proto-oncogene target sequences and acts as a transcriptional activator, *Oncogene*, **7**, 65–70.
36. Woods, D. B., Ghysdael, J., and Owen, M. J. 1992, Identification of nucleotide preferences in DNA sequences recognised specifically by c-Ets-1 protein, *Nucleic Acids Res.*, **20**, 699–704.
37. Merika, M. and Orkin, S. H. 1993, DNA-binding specificity of GATA family transcription factors, *Mol. Cell Biol.*, **13**, 3999–4010.
38. Nakai, K. and Horton, P. 1999, PSORT: a program for detecting sorting signals in proteins and predicting their subcellular localization, *Trends Biochem. Sci.*, **24**, 34–36.
39. Boehning, D. and Snyder, S. H. 2003, Novel neural modulators, *Annu. Rev. Neurosci.*, **26**, 105–131.
40. Burney, S., Tamir, S., Gal, A., and Tannenbaum, S. R. 1997, A mechanistic analysis of nitric oxide-induced cellular toxicity, *Nitric Oxide*, **1**, 130–144.
41. Kow, Y. W. 2002, Repair of deaminated bases in DNA, *Free Radic. Biol. & Med.*, **33**, 886–893.
42. Dedon, P. C. and Tannenbaum, S. R. 2004, Reactive nitrogen species in the chemical biology of inflammation, *Arch. Biochem. Biophys.*, **423**, 12–22.
43. Klinker, J. F. and Seifert, R. 1997, Functionally nonequivalent interactions of guanosine 5′-triphosphate, inosine 5′-triphosphate, and xanthosine 5′-triphosphate with the retinal G-protein, transducin, and with G_i-proteins in HL-60 leukemia cell membranes, *Biochem. Pharmacol.*, **54**, 551–562.
44. Seifert, R., Gether, U., Wenzel-Seifert, K., and Kobilka, B. K. 1999, Effects of guanine, inosine, and xanthine nucleotides on β_2-adrenergic receptor/G_s interactions: evidence for multiple receptor conformations, *Mol. Pharmacol.*, **56**, 348–358.
45. Liu, H. Y. and Seifert, R. 2002, Distinct interactions of $G_{s\alpha\text{-long}'}$, $G_{s\alpha\text{-short}'}$, and $G_{\alpha olf}$ with GTP, ITP, and XTP, *Biochem. Pharmacol.*, **64**, 583–593.
46. Cahill, P. A., Redmond, E. M., and Sitzmann, J. V. 2001, Endothelial dysfunction in cirrhosis and portal hypertension, *Pharmacol. Ther.*, **89**, 273–293.
47. Spirli, C., Fabris, L., Duner, E. et al. 2003, Cytokine-stimulated nitric oxide production inhibits adenylyl cyclase and cAMP-dependent secretion in cholangiocytes, *Gastroenterol.*, **124**, 737–753.
48. Trauner, M. 2003, When bile ducts say NO: the good, the bad, and the ugly, *Gastroenterol.*, **124**, 847–851.
49. Financsek, I., Mizumoto, K., and Muramatsu, M. 1982, Nucleotide sequence of the transcription initiation region of a rat ribosomal RNA gene, *Gene*, **18**, 115–122.
50. Oda, S., Nishida, J., Nakabeppu, Y., and Sekiguchi, M. 1995, Stabilization of cyclin E and cdk2 mRNAs at G1/S transition in Rat-1A cells emerging from the G0 state, *Oncogene*, **10**, 1343–1351.

Platelet-Derived Growth Factor-AA Is an Essential and Autocrine Regulator of Vascular Endothelial Growth Factor Expression in Non–Small Cell Lung Carcinomas

Yasunori Shikada,[1,2] Yoshikazu Yonemitsu,[1] Takaomi Koga,[1] Mitsuho Onimaru,[1] Toshiaki Nakano,[1] Shinji Okano,[1] Shihoko Sata,[1] Kazunori Nakagawa,[1] Ichiro Yoshino,[2] Yoshihiko Maehara,[2] and Katsuo Sueishi[1]

[1]Division of Pathophysiological and Experimental Pathology, Department of Pathology and [2]Department of Surgery and Science, Graduate School of Medical Sciences, Kyushu University, Fukuoka, Japan

Abstract

It is widely accepted that angiogenesis is required for tumor progression. Vascular endothelial growth factor (VEGF) is a key molecule for tumor angiogenesis; however, its expressional regulation is not well understood during all stages of tumorigenesis. Using cell lines and surgical specimens of human non–small cell lung cancers (NSCLCs), we here show that platelet-derived growth factor-AA (PDGF-AA) is an essential autocrine regulator for VEGF expression. To directly assess the expression of PDGF-AA–dependent VEGF and its roles in tumorigenesis, we stably transfected established cell lines with their antisense genes. In addition, the levels of PDGF-AA and VEGF expression in surgical sections were measured and compared with clinicopathologic findings such as tumor size and patient prognosis. PDGF-AA tightly regulated VEGF expression and had a greater effect on tumor size and patient prognosis than did VEGF in both cell lines and surgical sections. PDGF-AA expression was not seen in the atypical adenomatous hyperplasia at all, whereas VEGF was occasionally seen. Furthermore, the frequency of VEGF expression was higher in advanced NSCLCs than in precancerous lesions, which was tightly correspondent to the results for PDGF-AA. These results indicate that PDGF-AA is an important regulator of the frequency and level of VEGF expression during the transition from a precancerous lesion to advanced cancer. The PDGF-AA/VEGF axis, therefore, may be a ubiquitous autocrine system for enhancing angiogenic signals, and PDGF-AA, and its related pathways could be a more efficient target of antiangiogenic therapy for cancers than VEGF and its pathways. (Cancer Res 2005; 65(16): 7241-8)

Introduction

Angiogenesis is required for tumor progression, as supported by a number of studies showing a reduction in tumor growth by antiangiogenic agents (1–3). Folkman et al. proposed the concept of an "angiogenic switch" that is required for the progression to advanced cancer from an occult tumor (4). It is now widely accepted that the angiogenic switch is "off" when the effect of proangiogenic molecules is silent and "on" when the net balance is tipped in favor of angiogenesis (5, 6). Relatively less attention, however, has been paid to defining which molecule is the angiogenic switch or how it acts.

According to the original proposal (1), a molecule must have the following characteristics before it can be considered as a possible angiogenic switch: (a) it must be expressed specifically in advanced cancer but not in precancerous or early cancerous lesions of <2 mm^3; and (b) it must determine the size, and probably the malignant potentials, of cancers by controlling the expression of angiogenic growth factors. In the last decade, various signals that trigger tumor angiogenesis, including angiogenic factors, have been identified (7), and among these, vascular endothelial growth factor-A (VEGF-A, commonly called VEGF) has been recognized as one of the most potent mediators of tumor angiogenesis (8). A logical question followed: is VEGF an angiogenic switch for tumors? Unfortunately, this is not likely, because VEGF is abundantly expressed in cancers, precancerous lesions, and their originating tissue, although VEGF is essential for tumor angiogenesis and its frequency of expression is higher in advanced malignancies than in noncancerous tissue (9, 10). These theoretical considerations suggest the existence of upstream regulator(s) that mediate the expression of VEGF in tumors as molecular candidates for the angiogenic switch; however, the regulational mechanism of the expression of VEGF in each tumor has not been fully elucidated.

Several important studies have indicated that some oncogenes determining the malignant potentials of cancer, including Ras (11) and HER-2/*neu* (12), up-regulate VEGF expression, suggesting that the "angiogenic switch" might contain multiple molecules and signal transduction pathways. Furthermore, knowledge of important related mechanisms, such as that of the extracellular regulatory system for enhancing the expression of VEGF, is also limited.

Recently, we showed that the platelet-derived growth factor-AA (PDGF-AA)/PDGFα-receptor (PDGFRα)/p70S6K pathway in mesenchymal cells (fibroblasts and vascular smooth muscle cells) was essential for therapeutic and tumor angiogenesis *in vivo* (13). We also showed that PDGF-AA, which does not target the vascular endothelial cells, dominantly regulates the expression of VEGF, essentially contributing to the angiogenic process *in vivo* (13).

A previous study revealed that the expression of PDGF-AA is strictly limited in mesenchymal cells but not in cells of epithelial lineage, because of the methylation of GC-rich sequences of the *PDGF-A* promoter in epithelial cells (14). Demethylation can result in dysregulated expression of multiple genes and is now

---

Note: Supplementary data for this article are available at Cancer Research Online (http://cancerres.aacrjournals.org/).

The authors declare that they have no competing financial interests.

Requests for reprints: Yoshikazu Yonemitsu, Division of Pathophysiological and Experimental Pathology, Department of Pathology, Graduate School of Medical Sciences, Kyushu University, 3-1-1 Maidashi, Higashi-ku, Fukuoka 812-8582, Japan. Phone: 81-092-642-6064; Fax: 81-092-642-5965; E-mail: yonemitu@pathol1.med.kyushu-u.ac.jp.

doi:10.1158/0008-5472.CAN-04-4171

suggested to be an essential step for carcinogenesis (15, 16). These facts may support the hypothesis that a gain-of-function in cancers causes the dysregulated expression of PDGF-AA, which in turn causes the enhanced expression of VEGF by an autocrine mechanism, a system would be similar to that observed in mesenchymal cells. Using established cell lines and surgical specimens of non–small cell lung cancers (NSCLCs), which are a major cause of death in Western countries and Japan, we here show that PDGF-AA is a critical autocrine regulator for VEGF, which may be involved in the "angiogenic switch"–related pathways in malignancies.

Materials and Methods

Cells. The cancer cell lines, QG56 (human lung squamous cell carcinoma), A549 (human lung adenocarcinoma), and SAS and TF (human oral squamous cell carcinoma), were maintained in continuous culture in RPMI 1640 supplemented with 100 units/mL penicillin/streptomycin and 10% FCS. These cell lines were washed, and cell pellets were collected and then frozen in liquid nitrogen.

Reverse transcriptional-PCR. The gene expression of full-length *PDGF-A* was determined from MRC5 cells (a human fibroblast cell line). Total RNA of cultured cells growing exponentially was extracted using ISOGEN (Nippon Gene, Inc., Toyama, Japan) according to the manufacturer's protocol. Total RNA of clinical tissue was isolated using the same method. Synthesis of cDNA was done with 5.0 μg total RNA using a first-strand cDNA Synthesis Kit (Invitrogen Corp., Carlsbad, CA).

Construction of AS-PDGF-A/AS-VEGF plasmid. Primers incorporating the *Eco*RI site for PCR of PDGF-A were as follows: forward 5′-aaGAATTCatgaggaccttggcttgcctgc and reverse 5′-ttGAATTCttaggtgggttt-taacctttttctttt. PCR amplicons were directly inserted into a plasmid vector (PCR II) by the TA cloning method according to the manufacturer's protocol (Invitrogen). Gene expression was compared using the CEQ 2000 Sequence Detection System (Beckman Coulter, Inc., Fullerton, CA). The whole sequence was determined to be completely matched to a reported sequence (Genbank accession no. X03795). The amplicons were abstracted using an *Eco*RI restriction enzyme and then inserted into the vector for mammalian cell expression, pcDNA3.1(+) (Invitrogen).

The human VEGF165 cDNA expression plasmid vector was previously obtained (17). The *AS-VEGF* gene expression plasmid based on pcDNA3.1(+) was constructed as described above.

Establishment of stable transformant. Stable transfections were done using LipofectAMINE 2000 reagent (LF2000; Invitrogen) according to the manufacturer's instructions. Briefly, logarithmically growing cells were transfected with plasmid-LF2000 complex at a 1:2 weight ratio. Forty-eight hours later, the selective medium containing 0.5 mg/mL geneticin antibiotics (G418; Promega Corp., Madison, WI) was replaced, and the cell clones were selected and identified. Next, the transfected cells were spread onto 96-multiwell plates and cultured to confluence, and the cell clones that reduced PDGF-AA or VEGF expression were selected using the ELISA kit included in the Human PDGF-AA Immunoassay System and the ELISA kit included in the Human VEGF Immunoassay System, which detect VEGF121 and VEGF165 (both from R&D Systems, Inc., Minneapolis, MN).

The cell cloning was done thrice, and the cell clone showing the lowest PDGF-AA or VEGF expression in each cell line was used for experiments.

Immunoprecipitation. For immunoprecipitation, cells were lysed with 500 μL of cell lysis buffer (Promega) containing a cocktail of protease inhibitors (1.5 mmol/L pepstatin, 4 mmol/L leupeptin, 0.01 mol/L aprotinin, and 500 mmol/L phenylmethylsulfonyl fluoride), and the supernatant of the lysed cells was recovered for immunoprecipitation. The amount of protein was determined with a Protein Assay kit (Bio-Rad Laboratories, Inc., Hercules, CA), and aliquots of 500 μg of proteins were used for immunoprecipitation.

Nonspecific proteins bound to magnetic beads were eliminated by exposure to protein-G magnetic beads (Pharmacia Biotech AB, Uppsala, Sweden). For immunoprecipitation, 3 μg of anti-human PDGFRα antibody (R&D Systems) was added to the tube, bead pellets were heat treated in 20 mL mercaptoethanol sample buffer, and the samples were loaded onto 10% SDS-polyacrylamide gel. After transfer to the nitrocellulose membrane, immunoprecipitated proteins were determined by immunoblotting with polyclonal anti-phosphorylated-PDGFRα antibody (p-PDGFRα; Tyr^{720}, 1:100; Santa Cruz Biotechnology, Inc., Santa Cruz, CA).

Tissue samples. For immunohistochemistry, tissue samples were derived from 128 Japanese patients with NSCLC who underwent surgical resection at the Department of Surgery, Kyushu University Hospital (Fukuoka, Japan) between January 1990 and April 1995; for real-time quantitative PCR, samples were taken from 60 Japanese patients with NSCLC who underwent surgical resection in the same department between January 1996 and April 2000. No patient had received any antitumor treatment, including anticancer drugs or radiation therapy, before surgery.

Tumor and adjacent normal lung tissue samples were freshly obtained from resected lobes, immediately frozen in liquid nitrogen, and stored at −80°C for real-time PCR and reverse transcription-PCR (RT-PCR), or embedded in paraffin for immunohistochemistry after formalin fixation. All patients gave their informed consent before the tissue sampling.

Real-time quantitative PCR. Gene expression was measured using the ABI Prism 7000 Sequence Detection System (Perkin-Elmer Corp., Foster City, CA). The primer sequences were as follows: human PDGF-A, 636 bp, forward 5′-TCCACGCCACTAAGCATGTG-3′; reverse 5′-TCGACCTGACTCC-GAGGAAT-3′; probe 5′-FAM-CTGCAAGACCAGGACGGTCATTTACGA-TAMRA-3′; human VEGF, 574 bp, forward 5′-GAAGTGGTGAAGTTCATG-GATGTCTAT-3′; reverse 5′-TCAGGGTACTCCTGGAAGATGTC-3′; probe 5′-FAM-ACTGCCATCCAATCGAGACCCTGG-TAMRA -3′.

The coefficient of correlation was $\rho = 0.97$, and the slope was constant in each experiment. As internal controls, the same samples were tested for 18S rRNA (Perkin-Elmer) in the same manner. Each sample was analyzed in duplicate.

Immunohistochemistry. Formalin-fixed and paraffin-embedded tissue sections (diameter, 5 mm) were reacted overnight at 4°C with goat anti-PDGF-A antibody (1:65 in PBS, R&D Systems) or mouse anti-VEGF antibody (1:20 in PBS, R&D Systems) as primary antibodies. Isotype-matched nonimmune antibodies were used for negative controls. The rinsed sections were subjected to peroxidase-labeled secondary antibody (1:250 in PBS) at room temperature for 30 minutes. PDGF-A or VEGF protein was visualized using diaminobenzidine, and nuclei were counterstained with hematoxylin. A positive reaction was defined as immunohistochemical positivity in cells that showed a stronger reaction than that seen in arterial vascular smooth muscle cells in the same specimen, and in at least 30% of tumor cells at a ×200 high-power field for five randomly selected areas. All sections were examined by two independent investigators (Y.S. and T.K.) who were blinded to the clinical data.

For evaluation of angiogenesis, the dehydrated slides were treated with 40 mg/mL of proteinase K (DAKO, Carpinteria, CA) for 10 minutes at room temperature. After washing in PBS, they were treated with 3% H_2O_2 and then 5% nonfat dry milk, and incubated with von Willebrand factor (vWF, 1:800; DAKO) overnight at 4°C. The following procedures and visualization were done using the same methods described above. The microvessels in the tumor and adjacent mesenchyma, which was margined at 2-mm distant from the tumor periphery, were labeled with vWF under light microscopy.

Animals. Male BALB/c *nu/nu* mice (5 weeks old) were from Kyudo Co., Ltd. (Tosu, Saga, Japan). All animal experiments were done under approved protocols and in accordance with recommendations for the proper care and use of laboratory animals by the Committee for Animal, Recombinant DNA, and Infectious Pathogen Experiments at Kyushu University and according to the law (no. 105) and notification (no. 6) of the Japanese Government.

Tumor implantation model. With mice under sufficient anesthesia by an i.p. injection of sodium pentobarbital, 1×10^6 tumor cells were injected s.c. into the abdominal region. Measurement of the tumor was done thrice per week. Tumor volumes were estimated by the formula $V = \pi/6 \times a^2 \times b$, where a was the short and b was the long axis (11).

Statistical analysis. Results are presented as the mean ± SE. Differences between groups were determined by one-way ANOVA followed by an unpaired Student's t test with Bonferroni correction for multiple comparisons. The correlation between *PDGF-A* and *VEGF* was analyzed using Spearman's correlation analysis and κ-statistic analysis. Survival curves were plotted using the Kaplan-Meier's analysis, and the log-rank test was used to determine the statistical differences between life curves. The relationship between the expression of PDGF-AA and clinicopathologic factors was examined using the Mann-Whitney U test and Fisher's exact test, and a positive ratio with respect to tumor size was examined using the Cochran-Armitage linear trend test. The relationship between the microvessel count was also examined using the Mann-Whitney U test. $P < 0.05$ was considered significant.

Results

Platelet-derived Growth Factor-AA Is an Autocrine Regulator of Vascular Endothelial Growth Factor Expression in Human Non-Small Cell Lung Cancers

Established cell lines. To obtain direct evidence that PDGF-AA is an autocrine regulator for VEGF in human NSCLCs, we first established independent cell lines [i.e., QG56 (human lung squamous cell carcinoma) and A549 (human lung adenocarcinoma)] which were stably transfected with plasmid pcDNA3.1(+) expressing full-length antisense human *PDGF-A* cDNA (*AS-PDGFA*). Control lines transfected with an empty vector or full-length

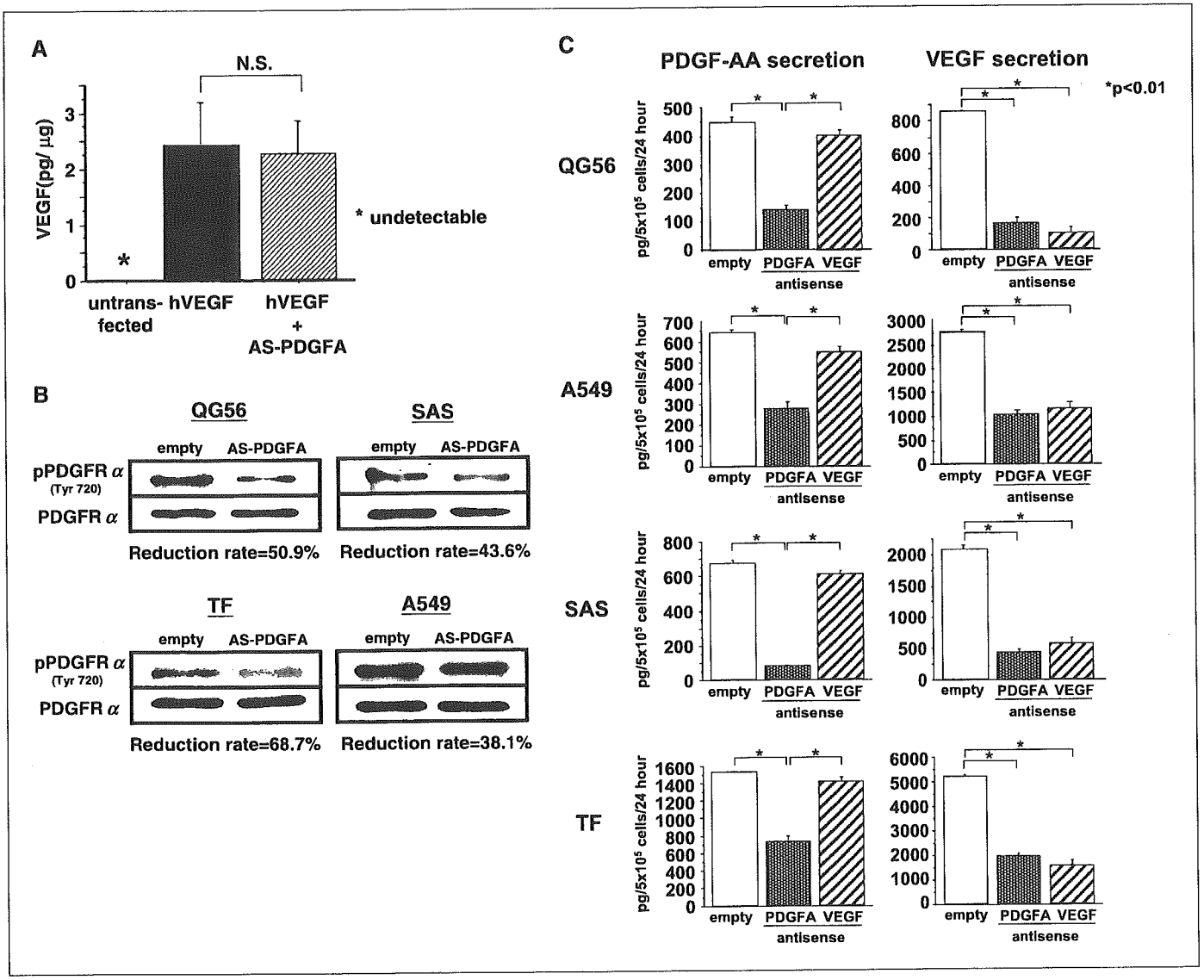

Figure 1. Specificity of *AS-PDGFA* for reduction of PDGFRα activity. *A*, *AS-PDGFA* transfection does not affect the expression of human *VEGF165* gene expression. Murine fibroblast (NIH3T3) was transfected with human *VEGF165* cDNA (hVEGF, *closed column*) or plasmid expressing antisense *PDGF-A* chain (AS-PDGFA), and culture medium 48 hours after gene transfer was subjected to human VEGF-specific ELISA. No reduction of VEGF expression by cotransfection of *AS-PDGFA* indicated any direct effect of *AS-PDGFA* to VEGF expression. *Columns*, averages of three independent experiments. *B*, reduction of phosphorylated PDGFRα caused by stable *AS-PDGFA* gene transfer in established cancer cell lines (QG56, A549, SAS, and TF). Stably transfected cells with *AS-PDGFA* or empty vector were established by the procedure described in Materials and Methods. Whole PDGFRα was immunoprecipitated and blotted by antibody for PDGFRα-specific phosphotyrosine (Tyr^{720}). The expression level of pPDGFRα was quantified by densitometry and standardized by nonphosphorylated PDGFRα, and the reduction rate was calculated. These experiments were done in duplicate and showed similar results. *C*, reduction of PDGF-AA secretion reduces the expression of VEGF in established cell lines. Establishment of cell lines (QG56, A549, SAS, and TF) with stably reduced PDGF-AA expression was described in Materials and Methods. After 24 hours of incubation without serum at 5×10^5 cells per well, the culture medium was subjected to ELISA for human PDGF-AA or VEGF. Each group contained $n = 3$. *Columns*, means; *bars*, ±SE. One-way ANOVA followed by an unpaired Student's t-test with Bonferroni correction for multiple comparison was done for statistical differences. *, $P < 0.01$.

antisense human *VEGF165* cDNA (AS-VEGF) were simultaneously established. In addition, two other cell lines, SAS and TF (human oral squamous cell carcinoma lines), were also included to confirm the findings. These cells were maintained in G418, and single-cell cloning was done thrice using 96-well plates. The clone that showed the lowest secretion of the target protein in each cell line was used for the following experiments.

A preliminary experiment showed high expressions of PDGF-AA and VEGF in all cell lines subjected to the ELISA (data not shown). Using murine fibroblasts (NIH3T3), we next examined whether *AS-PDGFA* might be cross-reactive for human VEGF expression, because the nucleotide sequence of *PDGF-A* showed ~30% homology to that of *VEGF*. *AS-PDGFA* transfection did not affect the protein secretion level from cotransfected sense human *VEGF165* expression vector [pcDNA3.1(+)/hVEGF165)] in the culture medium of NIH3T3 (Fig. 1*A*), indicating that *AS-PDGFA* did not seriously affect the expression of human VEGF.

All cell lines expressed the known receptor of PDGF-AA, PDGFRα, which was detected by RT-PCR (data not shown). This was also confirmed by immunoprecipitation to PDGFRα, and as expected, the phosphorylation of PDGFRα seemed lower in cells that were stably transfected with *AS-PDGFA* than in those transfected with an empty vector in repeated experiments; this finding was later confirmed by densitometry (Fig. 1*B*).

Furthermore, all cell clones stably transfected with *AS-PDGFA* showed significantly reduced PDGF-AA secretion, as well as reduced VEGF. On the other hand, transfection of AS-VEGF contributed only to the reduction of VEGF and not to the expression of PDGF-AA (Fig. 1*C*), indicating that PDGF-AA is an autocrine regulator for the expression of VEGF in these cell lines.

Surgical specimens. For further evidence regarding the role of PDGF-AA in VEGF expression, we did real-time quantitative RT-PCR to test the correlation of mRNA levels between *PDGF-A* chain and *VEGF* in surgically resected fresh NSCLC samples from 60 patients (adenocarcinoma, $n = 32$; squamous cell carcinoma, $n = 20$; others, $n = 8$). The expressions of *PDGF-A* mRNA and *VEGF* mRNA in the tumor were tightly correlated (Spearman's correlation test, $\rho = 0.838$, $P < 0.001$), and there was a similar finding in adjacent normal lung tissue (Spearman's correlation test, $\rho = 0.705$, $P < 0.001$; Fig. 2*A*), suggesting that similar to our previous findings in noncancerous mesenchymal cells, the expression of *PDGF-A* was correlated to that of *VEGF* in NSCLCs.

Further retrospective analysis by immunohistochemistry using 128 formalin-fixed tissue sections (adenocarcinoma, $n = 68$; squamous cell carcinoma, $n = 55$; others, $n = 5$) also supported these findings; the immunohistochemically positive reaction of PDGF-AA was tightly correlated with that of VEGF (Fig. 2*B* and *C*; κ-statistic analysis, $\kappa = 0.325$; $P = 0.0002$).

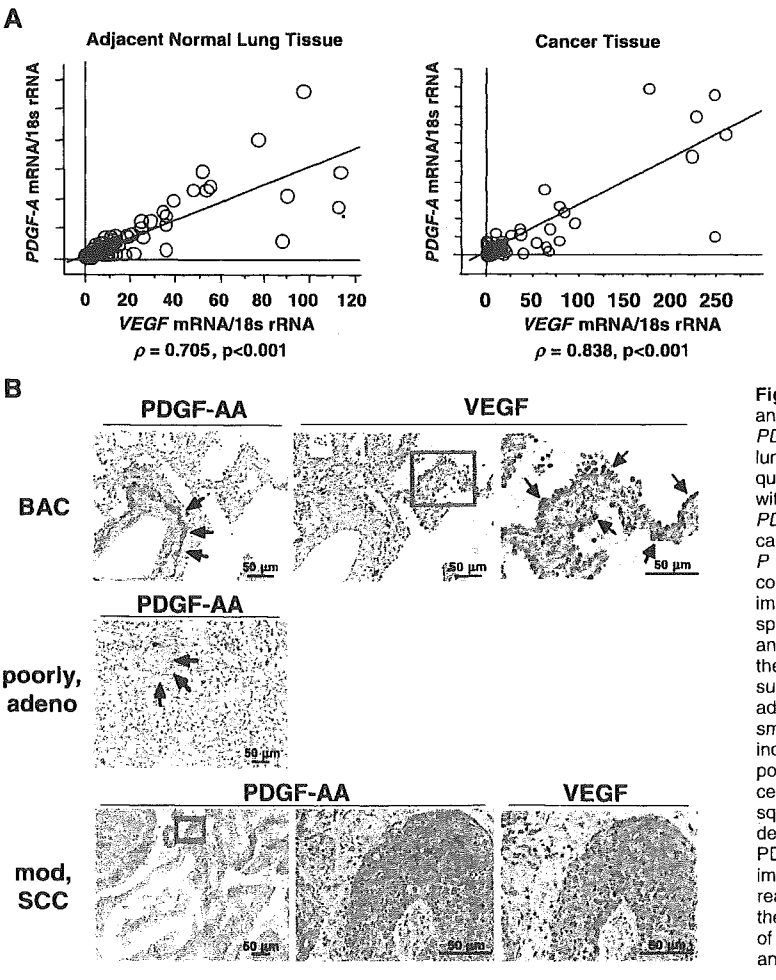

Figure 2. Correlation of expression of *PDGF-A* and *VEGF* mRNA and proteins in surgical specimens. *A*, correlation of mRNA between *PDGF-A* and *VEGF* in the surgical specimens of the adjacent normal lung tissue (*left*) and lung cancer tissue (*right*), assessed by quantitative real-time RT-PCR. Expression level was standardized with 18S rRNA as an internal control. Expression of mRNA of *PDGF-A* was tightly correlated with that of *VEGF* in the lung cancer tissue (Spearman's correlation analysis, $\rho = 0.838$, $P < 0.0001$), a finding seen in the normal lung tissue (Spearman's correlation analysis, $\rho = 0.705$, $P < 0.001$). *B*, representative immunohistochemical examination for PDGF-AA or VEGF in surgical specimens of NSCLCs. *Top*, negative case for PDGF-AA (*left*) and positive for VEGF (*middle* and *right*; *right*, high-powered view of the squared area of *middle*) in bronchioalveolar carcinoma (*BAC*) subtype. *Middle*, negative case for PDGF-AA in poorly differentiated adenocarcinoma (*poorly*, *adeno*). Note PDGF-AA-positive vascular smooth muscle cells in the arteries (*top left* and *middle*, *arrows*), indicating successful immunohistochemical reaction. *Bottom left*, positive case for PDGF-AA in moderately differentiated squamous cell carcinoma (*mod*, *SCC*); *bottom middle*, high-powered view of the squared area of (*bottom left*). *Bottom right*, serial section for detecting VEGF. *C*, relationship between immunoreactivities for PDGF-AA and VEGF. Positive reaction was defined as the immunohistochemically positive cells that showed a stronger reaction than that seen in arterial vascular smooth muscle cells in the same specimen, in at least 30% of tumor cells. Expression of PDGF-AA was tightly correlated with that of VEGF (κ-statistic analysis, $\kappa = 0.325$; $P = 0.0002$).

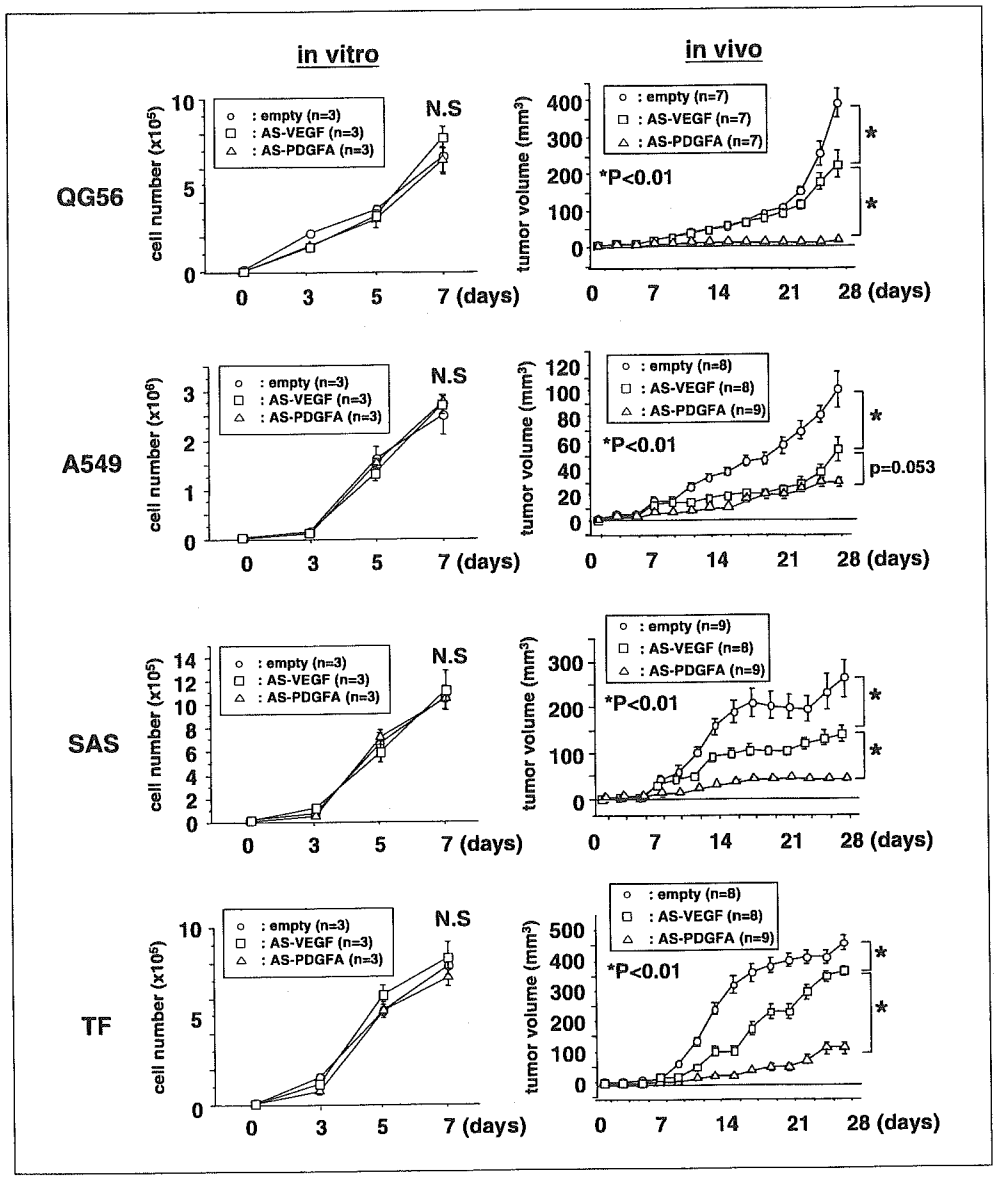

Figure 3. Significance of PDGF-AA and VEGF expression in tumor proliferation *in vitro* and in a tumor implantation model *in vivo*. *Left,in vitro*. Tumor cells (5×10^4 cells; QG56, A549, SAS, and TF) stably transfected with an empty plasmid, antisense *VEGF* (*AS-VEGF*), or antisense *PDGF-A* (*AS-PDGFA*) were spread on dish plate, and the number of tumor cells were counted at days 3, 5, and 7. No significant difference on the tumor proliferation was found in all groups. *Right, in vivo*. In turn, these tumor cells were s.c. injected into the abdominal wall, and the tumor growth was measured at each time point. *Points*, mean; *bars*, ±SE. Differences between the groups were compared using a one-way ANOVA followed by an unpaired Student's *t* test. *, $P < 0.01$.

Significance of Platelet-Derived Growth Factor-AA and Vascular Endothelial Growth Factor Expression in Human Non–Small Cell Lung Carcinomas

Established cell lines. We next returned to animal studies to examine the tumorigenesis in established cell lines. As a first step, we examined the proliferative activities of each cell transfected with an empty plasmid, *AS-PDGFA* or *AS-VEGF* and found no significant difference among the activities in any of the cell species (Fig. 3, *in vitro* experiment).

Reduction of VEGF expression resulted in mildly to moderately disturbed tumorigenesis in *nu/nu* mice in all four cell lines tested, as expected. On the other hand, stable transfection of *AS-PDGFA* caused considerably and significantly disturbed tumor growth in three of four cell lines, compared with those with an empty vector or *AS-VEGF* (Fig. 3, *in vivo* experiment). These results indicate that tumor growth is more dependent on the expression of PDGF-AA than that of VEGF.

We next assessed the tumor-induced angiogenesis *in vivo*, visualized by labeling with vWF, using tumor sections obtained at 28 days after tumor implantation (Fig. 4*A*, *arrows*, and *B*). None of the sections from QG56 tumor transfected with *AS-PDGFA* showed any histopathologic evidence of solid tumor; thus, these sections were excluded from the evaluation. In all tumor types, the number of intratumor microvessels was significantly decreased in the *AS-VEGF* group and even more significantly decreased in the *AS-PDGFA* group (Fig. 4*B*, *intratumor*). Similar findings were also observed for angiogenesis at the tumor periphery of SAS and TF tumors, but the effect was rather mild in A549 tumors (Fig. 4*B*, *peripheral*), probably reflecting the milder antitumor effect of antisense gene expression seen in Fig. 3.

Surgical specimens. Using 128 tissue sections immunohistochemically labeled for PDGF-AA (93 positive cases and 35 negative cases), we investigated the clinicopathologic role of PDGF-AA expression in NSCLCs. Among the clinicopathologic variables, only the tumor diameter was significantly larger in PDGF-AA-positive cases than in PDGF-AA-negative cases (Supplementary Table S1). Furthermore, as tumor size increased, the PDGF-AA-positive ratio was raised significantly (Cochran-Armitage test for linear trend, $P < 0.0001$), as was the VEGF-positive ratio (Cochran-Armitage test for linear trend, $P < 0.0001$;

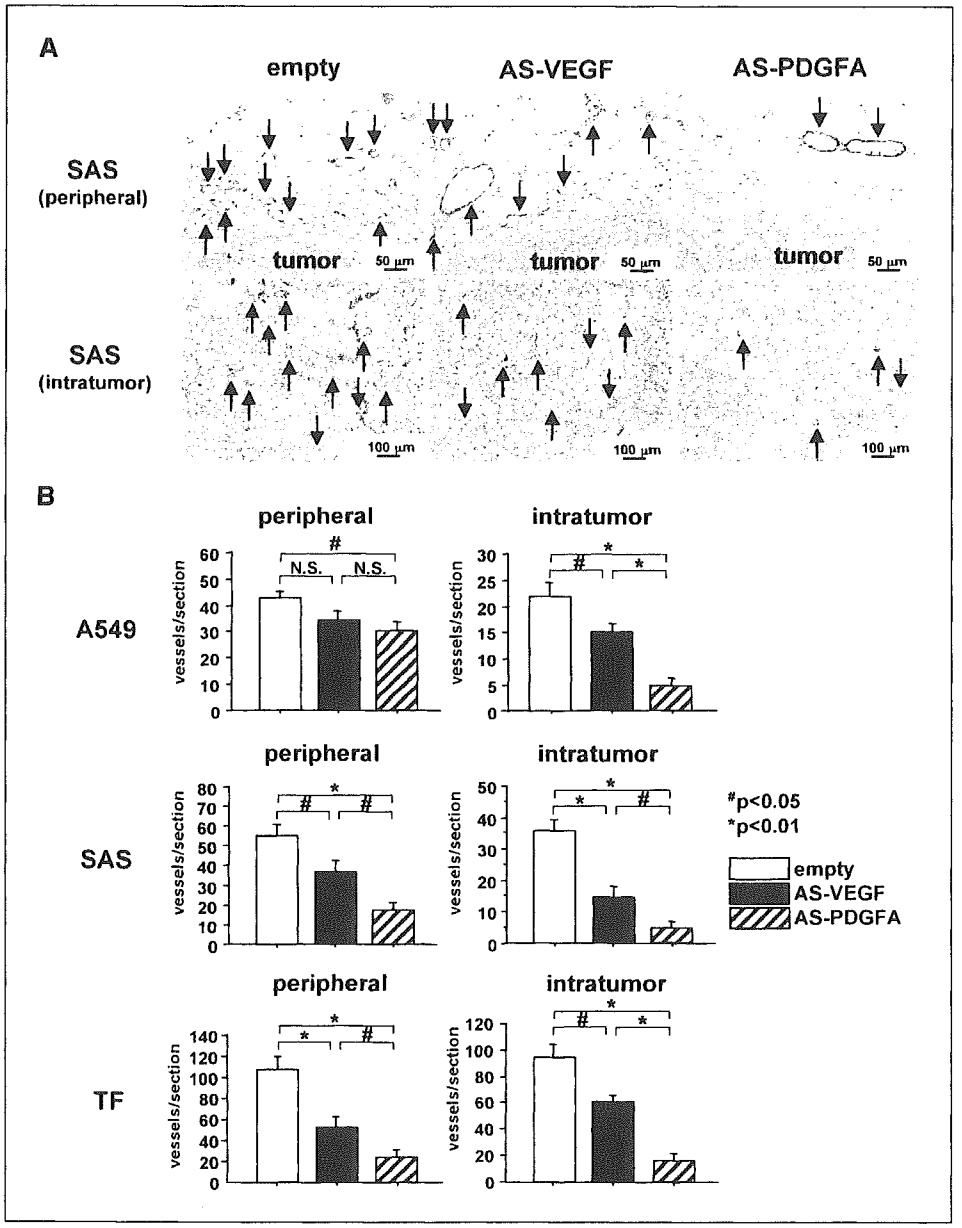

Figure 4. Immunohistochemical detection and quantification of microvessels in distinct part of tumors (tumor periphery and intratumor). Tumors shown in Fig. 4 were obtained at 28 days after implantation, and the sections from these were subjected to immunohistochemical examination for von Willebrand factor (*vWF*). QG56 was excluded from this analysis, because no apparent viable tumor could be found in this type of tumor transfected with *AS-PDGFA*. *A*, representative immunohistochemical findings of microvessels (*arrows*) in SAS tumors located at <2 mm from tumor periphery (*peripheral, top*) and at intratumor (*intratumor, bottom*). Note the marked reduction of the number of microvessels, especially in the tumor with *AS-PDGFA*. Counterstained with hematoxylin. *B*, quantitative analysis of the number of microvessels located at the tumor periphery or intratumor in each tumor type.

Table 1). Interestingly, all tissue sections of noninvasive adenocarcinoma, bronchioalveolar carcinoma (n = 7; all cases were included in $20 \leq \phi < 30$), and high-grade atypical adenomatous hyperplasia (AAH, n = 13), which are now considered to be precancerous lesions (18, 19), were negative for PDGF-AA. The seven cases of bronchioalveolar carcinoma included three VEGF-positive cases (42.9%). These results thus indicate that the expression of PDGF-AA may be essentially related to the size and progression of tumors.

Finally, a comparison of the 5-year survival rates of patients with NSCLCs who were VEGF positive (81 cases) or negative (47 cases) did not show a significant difference between the two groups (Fig. 5*A*; 38.6%, confidence interval [CI] = 15.6 versus 43.6%, CI = 11.6, respectively), whereas that of patients who were PDGF-A positive was significantly lower than that of those with a negative reaction ($P < 0.05$; Fig. 5*B*; 36.1%, CI = 17.8 versus 56.5%, CI = 11.0, respectively).

Discussion

The key observations obtained in the present study were as follows: (a) similar to our earlier observations in noncancerous mesenchymal cells, PDGF-AA was found to be an autocrine regulator for VEGF in NSCLCs, indicating that the PDGF-AA/VEGF axis may be a ubiquitous autocrine system for enhancing angiogenic signals; (b) the expression level of PDGF-AA was more critical for experimental tumor growth than that of VEGF *in vivo*, and the expression of PDGF-AA was rarely seen in precancerous or early cancer lesions of surgical sections; and (c) PDGF-AA expression was a prognostic indicator for individuals with NSCLCs. These results strongly suggest that PDGF-AA and its related pathways may be a more efficient target of antiangiogenic therapy for cancers than VEGF and its related pathways.

Recent studies have identified various signals related to tumor angiogenesis, including metabolic and/or mechanical stress, immune/inflammatory response, and factors that genetically

Table 1. Relationship between PDGF-AA/VEGF expression and tumor diameter of human NSCLCs

Diameter	AAH (n = 13)	Tumor diameter (ϕ) of NSCLCs (n = 128)				
		ϕ < 20 (n = 5)	20 ≤ ϕ < 30 (n = 21*)	30 ≤ ϕ < 40 (n = 31)	40 ≤ ϕ < 50 (n = 30)	50 ≤ ϕ (n = 41)
PDGF-AA-positive rate (%)†	0 (0.0)	2 (40.0)	12 (57.1)	19 (61.3)	24 (80.0)	36 (87.8)
VEGF-positive rate (%)‡	4 (30.7)	2 (40.0)	9 (42.8)	18 (58.0)	21 (70.0)	31 (75.6)

*Includes seven bronchioaveolar carcinomas.
†P < 0.0001, Cochran-Armitage test for trend.
‡P < 0.001, Cochran-Armitage test for trend.

activate oncogenes and control the production of angiogenic regulators such as VEGF, angiopoietins, fibroblast growth factors, hepatocyte growth factor, etc. (7). There is no longer doubt that these signals contribute to tumor progression; however, relatively less attention has been paid to the critical question of which molecules and signal transduction pathways are critically involved in the angiogenic switch and how they function.

VEGF is an essential mediator for tumor angiogenesis, and that conclusion has been supported by the findings of a number of experimental and clinical studies, including promising early results of a humanized anti-VEGF antibody, Avastin (20–22). VEGF, however, is not likely to meet the definition of an angiogenic switch, and this assertion was supported by the present finding that AAH occasionally expressed VEGF (Table 1). Therefore, we should be able to identify an upstream regulator that controls the expression of VEGF in tumors. In the current study, we identified PDGF-AA as a possible candidate for one of the molecules involved to the angiogenic switch that meets the definition noted above, and the relationship between the role of PDGF-AA and tumorigenesis has been summarized in Supplementary Fig. S1A.

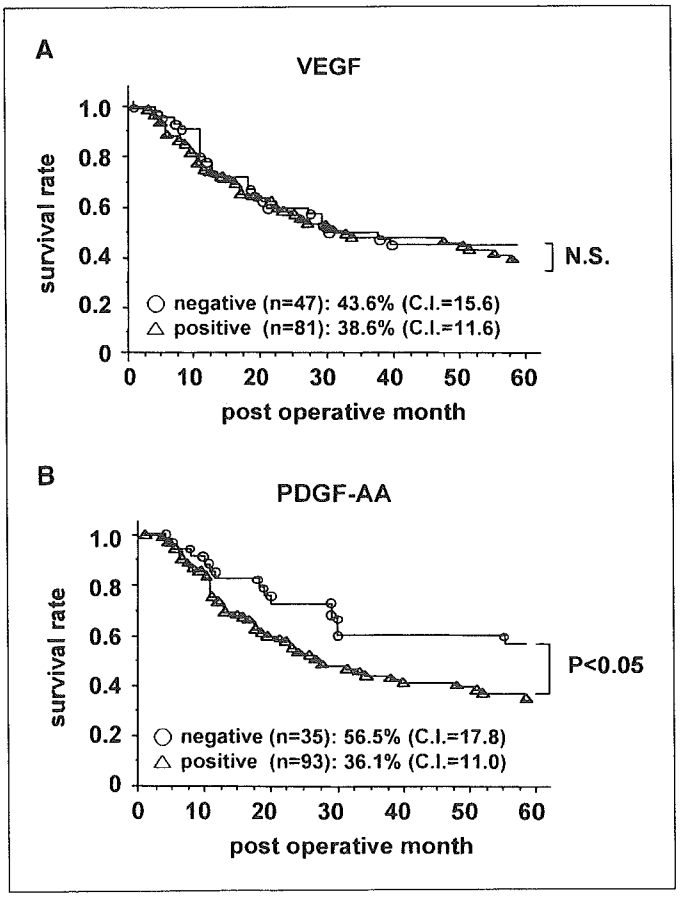

Figure 5. Comparison of 5-year survival of patients with NSCLCs. Kaplan-Meier curves indicating a 5-year survival of patients with VEGF-positive or -negative cases (*A*), PDGF-A-positive or PDGF-A-negative cases (*B*). The log-rank test was used to determine the statistical differences between life curves. A probability value of P < 0.05 was considered significant.

A tumor implantation assay indicated that inhibition of tumor growth was more pronounced in *AS-PDGFA* than in *AS-VEGF*, suggesting that the expression of PDGF-AA may not only contribute to the regulation of VEGF but also exert other effects on tumor progression. With regard to tumor angiogenesis, we hypothesize that (a) in addition to VEGF, PDGF-AA may regulate other factors advantageous to tumor growth, including other angiogenic factors; and (b) in addition to the indirect angiogenic effect using VEGF, PDGF-AA itself may directly contribute to the angiogenic responses. At present, little is known regarding the former point, which we are currently investigating via microarray analysis. The latter point may be supported by our previous study indicating that PDGF-AA stimulates and maintains the local VEGF expression in mesenchymal cells (13). Such a paracrine mechanism of PDGF-AA for angiogenesis, which is supported by several studies (23–27), may reflect the difference of tumor growth between *AS-PDGFA* and *AS-VEGF*. From this point of view, PDGF-AA is likely to be an autocrine and paracrine angiogenic switch in solid tumors (Supplementary Fig. S1*B*). Regarding the nonangiogenic actions, the paracrine mode of PDGF-AA causes a desmoplastic reaction (28), which is an important feature of advanced NSCLCs (29), by activating mesenchymal myofibroblasts.

Might a PDGF-AA-related signal transduction pathway be a more effective molecular target for antitumor therapy than a pathway related to VEGF? Although it seems premature to draw such a conclusion, the current study suggests this possibility, and some recent studies may also support it. For example, in a previous study that measured the levels of various angiogenic factors, including VEGF, in the tumors of neuroblastoma patients, only the expression level of PDGF-AA was significantly correlated to patient survival, even when a high level of expression of various angiogenic factors was detected (30). On the other hand, an inhibitor of tyrosine kinases, including PDGFRs, is likely to be effective in patients with malignant tumors (31), suggesting that PDGF-AA and its related pathways may be important targets for tumor

angiogenesis. Among these tyrosine kinases, it has been suggested in a recent experimental study that PDGF-AA and PDGFRα might be one of the essential regulators for tumor angiogenesis (32); some thalidomide analogues markedly inhibited tumor growth and angiogenesis *in vivo* via a marked reduction of PDGF-AA without apparent changes of the expression levels of other angiogenesis-related factors. Together, these findings strongly suggest that the PDGF-AA/PDGFRα signal transduction pathway warrants further study for the potential treatment of patients with intractable malignancies.

An important limitation of the present study was the lack of direct evidence of the demethylation status of the *PDGF-A* promoter in NSCLCs; because of this, the scheme shown in Supplementary Fig. S1*A* is still hypothetical, not definitive. For precise assessment regarding this issue, careful laser dissection of cancer cells should be done without contamination of mesenchymal cells, because the *PDGF-A* promoter of nontumorous mesenchymal cells should be demethylated. We have started this delicate assessment, and the data will be available in the near future.

In conclusion, we identified PDGF-AA as an autocrine, and probably a paracrine, regulator that made an essential contribution to the expression of VEGF in NSCLCs, affecting tumorigenesis revealed by experimental and clinicopathologic studies. Therefore, PDGF-AA and its related pathways, which determine the expression of VEGF in tumors, may have potential as molecular targets in an antitumor strategy for disrupting tumor angiogenesis.

Acknowledgments

Received 11/22/2004; revised 5/23/2005; accepted 5/31/2005.

Grant support: Japanese Ministry of Education, Culture, Sports, Science, and Technology grant-in-aid (Y. Yonemitsu and K. Sueishi) and Organization for Pharmaceutical Safety and Research Grant for the Promotion of Basic Science Research in Medical Frontiers project No. MF-21 (Y. Yonemitsu and K. Sueishi).

The costs of publication of this article were defrayed in part by the payment of page charges. This article must therefore be hereby marked *advertisement* in accordance with 18 U.S.C. Section 1734 solely to indicate this fact.

We thank Drs. N. Kinukawa and J. Tsuchihashi for their help with the statistical analysis and Chie Arimatsu for her help with the animal experiments.

References

1. Folkman J. Tumor angiogenesis: therapeutic implications. N Engl J Med 1971;285:1182–6.
2. Hlatky L, Hahnfeldt P, Folkman J. Clinical application of antiangiogenic therapy: microvessel density, what it does and doesn't tell us. J Natl Cancer Inst 2002;94:883–93.
3. Holmgren L, O'Reilly MS, Folkman J. Dormancy of micrometastases: balanced proliferation and apoptosis in the presence of angiogenesis suppression. Nat Med 1995;1:149–53.
4. Kandel J, Bossy-Wetzel E, Radvanyi F, Klagsbrun M, Folkman J, Hanahan D. Neovascularization is associated with a switch to the export of bFGF in the multistep development of fibrosarcoma. Cell 1991;66:1095–104.
5. Bouck N, Stellmach V, Hsu SC. How tumors become angiogenic. Adv Cancer Res 1996;69:135–74.
6. Hanahan D, Weinberg RA. The hallmarks of cancer. Cell 2000;100:57–70.
7. Carmeliet P, Jain RK. Angiogenesis in cancer and other diseases. Nature 2000;407:249–57.
8. Ferrara N, Alitalo K. Clinical applications of angiogenic growth factors and their inhibitors. Nat Med 1999;5:1359–64.
9. Baillie R, Carlile J, Pendleton N, Schor AM. Prognostic value of vascularity and vascular endothelial growth factor expression in non-small cell lung cancer. J Clin Pathol 2001;54:116–20.
10. Liao M, Wang H, Lin Z, Feng J, Zhu D. Vascular endothelial growth factor and other biological predictors related to the postoperative survival rate on non-small cell lung cancer. Lung Cancer 2001;33:125–32.
11. Lazarov M, Kubo Y, Cai T, et al. CDK4 coexpression with Ras generates malignant human epidermal tumorigenesis. Nat Med 2002;8:1105–14.
12. Laughner E, Taghavi P, Chiles K, Mahon PC, Semenza GL. HER2 (neu) signaling increases the rate of hypoxia-inducible factor 1α (HIF-1α) synthesis: novel mechanism for HIF-1-mediated vascular endothelial growth factor expression. Mol Cell Biol 2001;21:3995–4004.
13. Tsutsumi N, Yonemitsu Y, Shikada Y, et al. Essential role of PDGFRα-p70S6K signaling in mesenchymal cells during therapeutic and tumor angiogenesis *in vivo*: role of PDGFRα during angiogenesis. Circ Res 2004;94:1186–94.
14. Lin XH, Guo C, Gu LJ, Deuel TF. Site-specific methylation inhibits transcriptional activity of platelet-derived growth factor A-chain promoter. J Biol Chem 1993;268:17334–40.
15. Chen RZ, Pettersson U, Beard C, Jackson-Grusby L, Jaenisch R. DNA hypomethylation leads to elevated mutation rates. Nature 1998;395:89–93.
16. Di.Croce L, Raker VA, Corsaro M, et al. Methyltransferase recruitment and DNA hypermethylation of target promoters by an oncogenic transcription factor. Science 2002;295:1079–82.
17. Yonemitsu Y, Kaneda Y, Morishita R, Nakagawa K, Nakashima Y, Sueishi K. Characterization of *in vivo* gene transfer into the arterial wall mediated by the Sendai virus (HVJ)-liposomes: an effective tool for the *in vivo* study of arterial diseases. Lab Invest 1996;75:313–23.
18. Koga T, Hashimoto S, Sugio K, et al. Lung adenocarcinoma with bronchioloalveolar carcinoma component is frequently associated with foci of high-grade atypical adenomatous hyperplasia. Am J Clin Pathol 2002;117:464–70.
19. Mori M, Chiba R, Takahashi T. Atypical adenomatous hyperplasia of the lung and its differentiation from adenocarcinoma. Characterization of atypical cells by morphometry and multivariate cluster analysis. Cancer 1993;72:2331–40.
20. Herbst RS, Sandler AB. Non-small cell lung cancer and antiangiogenic therapy: what can be expected of bevacizumab? Oncologist 2004;9:S19–26.
21. Johnson DH, Fehrenbacher L, Novotny WF, et al. Randomized phase II trial comparing bevacizumab plus carboplatin and paclitaxel with carboplatin and paclitaxel alone in previously untreated locally advanced or metastatic non-small cell lung cancer. J Clin Oncol 2004;22:2184–91.
22. Sandler AB, Johnson DH, Herbst RS. Anti-vascular endothelial growth factor monoclonals in non-small cell lung cancer. Clin Cancer Res 2004;10:4258–62.
23. Cao R, Brakenhielm E, Li X, et al. Angiogenesis stimulated by PDGF-CC, a novel member in the PDGF family, involves activation of PDGFR-αα and -αβ receptors. FASEB J 2002;16:1575–83.
24. Marx M, Perlmutter RA, Madri JA. Modulation of platelet-derived growth factor receptor expression in microvascular endothelial cells during *in vitro* angiogenesis. J Clin Invest 1994;93:131–9.
25. Metheny-Barlow LJ, Flynn B, van Gijssel HE, Marrogi A, Gerwin BI. Paradoxical effects of platelet-derived growth factor-A overexpression in malignant mesothelioma. Antiproliferative effects *in vitro* and tumorigenic stimulation *in vivo*. Am J Respir Cell Mol Biol 2001;24:694–702.
26. Oikawa T, Onozawa C, Sakaguchi M, Morita I, Murota S. Three isoforms of platelet-derived growth factors all have the capability to induce angiogenesis *in vivo*. Biol Pharm Bull 1994;17:1686–8.
27. Risau W, Drexler H, Mironov V, et al. Platelet-derived growth factor is angiogenic *in vivo*. Growth Factors 1992;7:261–6.
28. Shao ZM, Nguyen M, Barsky SH. Human breast carcinoma desmoplasia is PDGF initiated. Oncogene 2000;19:4337–45.
29. Matsuo Y, Hashimoto S, Koga T, et al. Growth pattern correlates with the distribution of basement membrane and prognosis in lung adenocarcinoma. Pathol Res Pract 2004;200:517–29.
30. Eggert A, Ikegaki N, Kwiatkowski J, Zhao H, Brodeur GM, Himelstein BP. High-level expression of angiogenic factors is associated with advanced tumor stage in human neuroblastomas. Clin Cancer Res 2000;6:1900–8.
31. George D. Platelet-derived growth factor receptors: a therapeutic target in solid tumors. Semin Oncol 2001;28:S27–33.
32. Ng SS, MacPherson GR, Gutschow M, Eger K, Figg WD. Antitumor effects of thalidomide analogs in human prostate cancer xenografts implanted in immunodeficient mice. Clin Cancer Res 2004;10:4192–7.

Journal of Pathology
J Pathol 2005; **207**: 410–421
Published online 21 September 2005 in Wiley InterScience (www.interscience.wiley.com). **DOI:** 10.1002/path.1848

Original Paper

Frequent alteration of *p16*^{INK4a}/*p14*^{ARF} and *p53* pathways in the round cell component of myxoid/round cell liposarcoma: *p53* gene alterations and reduced p14^{ARF} expression both correlate with poor prognosis

Yoshinao Oda,[1]* Hidetaka Yamamoto,[1] Tomonari Takahira,[1] Chikashi Kobayashi,[1] Kenichi Kawaguchi,[1] Naomi Tateishi,[1] Yoko Nozuka,[1] Sadafumi Tamiya,[1] Kazuhiro Tanaka,[2] Shuichi Matsuda,[2] Ryohei Yokoyama,[3] Yukihide Iwamoto[2] and Masazumi Tsuneyoshi[1]#

[1]*Department of Anatomic Pathology, Graduate School of Medical Sciences, Kyushu University, Fukuoka, Japan*
[2]*Department of Orthopaedic Surgery, Graduate School of Medical Sciences, Kyushu University, Fukuoka, Japan*
[3]*Division of Orthopaedic Surgery, National Kyushu Cancer Center, Fukuoka, Japan*

*Correspondence to: Yoshinao Oda, Department of Anatomic Pathology, Graduate School of Medical Sciences, Kyushu University, 3-1-1 Maidashi, Higashi-ku, Fukuoka 812-8582, Japan. E-mail: oda@surgpath.med.kyushu-u.ac.jp

#Reprint requests to: Masazumi Tsuneyoshi, Department of Anatomic Pathology, Graduate School of Medical Sciences, Kyushu University, 3-1-1 Maidashi, Higashi-ku, Fukuoka 812–8582, Japan. E-mail: masazumi@surgpath.med.kyushu-u.ac.jp.

Received: 27 April 2005
Revised: 15 June 2005
Accepted: 8 July 2005

Abstract

In myxoid/round cell liposarcoma (MLS/RCLS), the presence of a round cell (RC) component has been reported to correlate with a worse prognosis for the patients. However, little is known about the molecular genetic differences between conventional myxoid (MX) components and RC components in this tumour. The aim of this study was to investigate the possible implications of molecular alterations of G_1 to S-phase check-point genes, especially in the RC component. We evaluated the immunohistochemical expression of p53, MDM2, p14 and p16 protein and assessed proliferative activities using MIB-1 in 29 RC components and 81 MX components from 90 cases. Mutation of the *p53* gene, amplification of the *MDM2* gene, homozygous deletion, methylation status and mutation of the *p16*^{INK4a}/*p14*^{ARF} genes were also investigated, using concordant paraffin-embedded and frozen material. The data were analysed together with clinicopathological factors to assess their prognostic implications in MLS/RCLS. Immunohistochemically, the over-expression of p53 protein ($p = 0.01366$) and the reduced expression of p14 ($p < 0.0001$) and p16 ($p < 0.0001$) proteins were significantly more frequently observed in RC components than in MX components. Reduced expression of p14 protein correlated significantly with hypermethylation of the *p14*^{ARF} gene promoter ($p = 0.0176$) and over-expression of p53 protein ($p = 0.00837$). By univariate analysis, reduced expression of p14 and *p53* missense mutation were found to reduce the rate of survival significantly ($p < 0.05$). Multivariate analysis, including clinicopathological factors, revealed that tumour site ($p = 0.0251$), the presence of an RC component ($p = 0.0113$), high MIB-1 labelling index ($p = 0.0005$) and *p53* missense mutation ($p = 0.0036$) were adverse prognostic factors. In MLS/RCLS, reduction of p14 protein expression and *p53* mutation were related to poor prognosis. Accordingly, the p14^{ARF}/p53 pathway may contribute to the presence of an RC component and malignant progression in this tumour.

Keywords: **myxoid/round cell liposarcoma; p53; *p14*^{ARF}; *p16*^{INK4a}; prognosis**

Introduction

Myxoid/round cell liposarcoma (MLS/RCLS) is the second most common subtype of liposarcoma and represents about 10% of all adult soft tissue sarcomas [1]. The existence of a morphological spectrum in which purely myxoid (MX) and round cell (RC) liposarcoma represent well and poorly differentiated components, respectively, is supported by the presence of the same cytogenetic alterations and the *TLS–CHOP* fusion gene in both components [2–4]. However, a subset of MLS/RCLS shows histological progression from typical MX features to RC morphology, a finding that has been reported to be associated with a significantly worse prognosis [1,5–11].

The *p16*^{INK4a}/*p14*^{ARF} locus on the short arm of chromosome 9 is one of the most frequently altered sequences in human cancer. Activation of p16^{INK4} and p14^{ARF} results in blockage of cell-cycle progression and inhibition of cellular proliferation. Mutational or transcriptional inactivation of the *p16*^{INK4a}/*p14*^{ARF} gene has been reported in several kinds of carcinoma, as well as in bone and soft tissue sarcomas, by either homozygous deletion, mutation or methylation of the

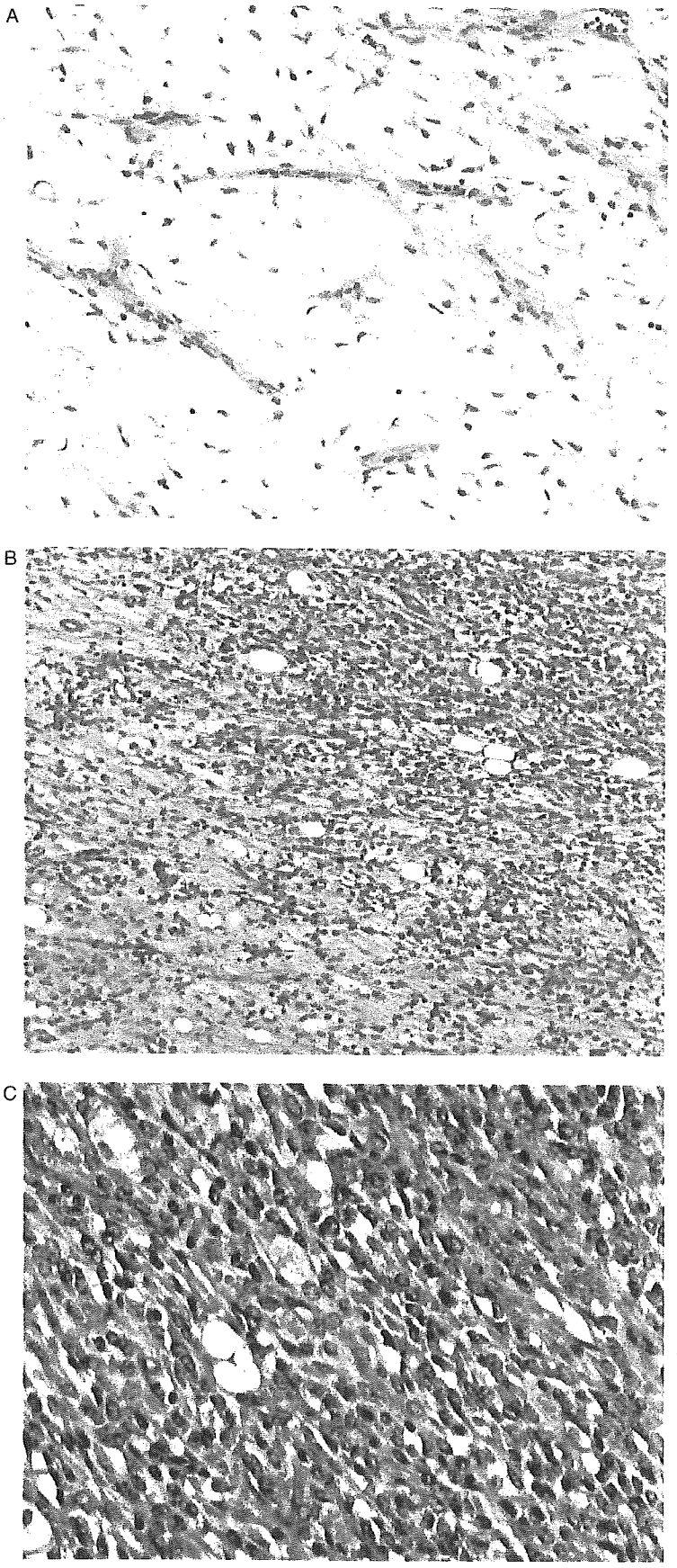

Figure 1. (A) Myxoid component in myxoid/round cell liposarcoma. This component shows scattered lipoblasts at varying stages with abundant myxoid matrix and arborizing vasculature. (B) Transition between myxoid component (lower left) and round cell component (upper right). (C) Round cell component composed mainly of undifferentiated round cells without stroma, accompanied by a few lipoblasts

Table 1. Monoclonal antibodies used in immunohistochemical studies

Antibody	Clone	Type	Source	Dilution	Pretreatment
p53	Pab 1801	Monoclonal	Oncogene Research Products, Boston, MA	1:100	10 min microwave
MDM2	IF2	Monoclonal	Oncogene Research Products	1:40	20 min microwave
$p14^{ARF}$	FL132	Polyclonal	Santa Cruz Biotechnology, Santa Cruz, CA	1:100	20 min microwave
p16	F12	Monoclonal	Santa Cruz Biotechnology	1:50	20 min microwave
Ki-67	MIB-1	Monoclonal	Immunotech, Marseilles, France	1:100	20 min microwave

promoter region [12–23]. This $p16^{INK4a}/p14^{ARF}$ gene cluster is an important tumour suppressor gene that plays an important role in the p53 and pRb cell-cycle pathways [24]. Recently, deregulation of the TP53/$p14^{ARF}$ pathway has been reported in astrocytoma [25] and meningioma [26].

In this study we first performed clinicopathological analysis in 120 cases of MLS/RCLS. Then, alterations in expression of $p16^{INK4}$, $p14^{ARF}$, p53 and MDM2 proteins, as well as proliferative activity, were examined by immunohistochemistry in 90 cases and their expression in the MX and RC components was compared. Furthermore, genetic changes of $p16^{INK4a}/p14^{ARF}$ and *p53* tumour suppressor genes were screened in both components and examined to establish whether the aberrations of these genes or gene products may play a role in the malignant progression or biological behaviour of this tumour.

Materials and methods

Tissue samples

The study protocol was approved by the Institutional Ethics Committee in Kyushu University (No. 177). The diagnosis of MLS/RCLS was defined according to the World Health Organization classification from 2002 [1] and Weiss and Goldblum's criteria [10] (Figure 1). A total of 120 cases of MLS/RCLS were retrieved from our soft tissue tumour file from the years 1971–2003. The number of histological slides evaluated ranged from one to 24, with a mean of five slides per case. The histological definition of an RC component was that the cells had acquired a round shape and had overlapping nuclei, such that one could easily identify clusters of cells sitting back to back. The percentage occupied by the RC component was estimated by scanning all the individual sections from each tumour. All of the patients had been treated by marginal or wide resection. Histological tumour grade was evaluated according to the French Federation of Cancer Centres (FNCLCC) grading system [27]. Each case was also evaluated according to the American Joint Committee on Cancer (AJCC) grading system [28], whenever possible.

Immunohistochemistry

Blocks were selected from areas that contained both MX and RC components, except in those cases where the tumour was composed entirely of only MX or RC areas. Consequently, we evaluated immunohistochemical profiles in 110 components, comprising 29 RC components and 81 MX components from 90 available cases.

For immunohistochemical study, 4 μm sections were stained using a streptavidin–biotin–peroxidase method (Histofine; Nichirei, Tokyo, Japan). The primary antibodies used in this study are summarized in Table 1. For p53 and MDM2, staining of >10% of the nuclei was required for a case to be scored positive. Each case was scored for p16 immunoreactivity using previously published criteria [29]. The immunoreactivity for p14 was evaluated by the same method as that used for p16. The labelling indices (LI) for MIB-1 were determined by counting the positively-stained nuclei in at least 500 tumour cells in both MX and RC components. When comparing the correlation between MIB-1 LI and patient prognosis, the higher MIB-1 LI was chosen in each case.

DNA extraction

The paraffin sections were stained lightly with haematoxylin for ease of identification. Different areas of pure myxoid components and round cell components were cut from the sections, using disposable sterile fine needles under a microscope, and placed in microtubes. Genomic DNA was extracted using the standard proteinase K digestion and phenol/chloroform extraction methods. In total, 98 DNA samples from 23 RC components and 75 MX components were prepared from 81 cases. From among these 98 samples, 23 DNA samples were also prepared from 23 cases of concordant frozen material.

Mutational analysis of the $p16^{INK4a}/p14^{ARF}$ and *p53* genes by polymerase chain reaction–single-strand conformation polymorphism (PCR-SSCP)

Mutational analysis was performed for the $p16^{INK4a}/p14^{ARF}$ (exons 1α, 1β, 2, 3) and *p53* (exons 5–9) genes. Primer sequences and PCR conditions were the same as those previously described [19,30–33]. SSCP and direct sequencing were carried out as previously described [22,31].

Differential PCR assay for the homozygous deletion of $p16^{INK4a}/p14^{ARF}$ genes and *MDM2* gene amplification

The differential PCR method for detecting homozygous deletion of exons 1α and 1β of $p16^{INK4a}/p14^{ARF}$

was based on a modification of reported methods using β-actin or the *GAPDH* gene as the internal control [22,30,33]. The level of *MDM2* amplification was determined by comparing the ratio of the intensities of the *MDM2* and *PAH* PCR products for each of the samples, as previously described [31].

Methylation-specific PCR (MSP) for the promoter region of the $p16^{INK4a}/p14^{ARF}$ genes

Bisulphite modification was performed using the CpGenome DNA Modification Kit (Intergen, New York, NY). MSP was performed to determine the DNA methylation status of CpG islands of the promoter region of the $p16^{INK4a}$ and $p14^{ARF}$ genes. The primer pairs used in this study have been described previously [32].

Statistical analysis

Fisher's exact test was used to evaluate the association between the two dichotomous variables. The difference in the MIB-1 LI between two groups was estimated by an unpooled *t*-test. Survival curves were calculated by the Kaplan–Meier method, and survival differences were evaluated by log-rank test. Multivariate survival analysis was performed using the Cox proportional hazards regression model.

Results

Clinicopathological findings

The clinicopathological data are summarized in Table 2. The 120 patients (61 men, 59 women) with MLS/RCLS were in the age range 18–83 years (average 46.4 years). Follow-up information was available for 102/120 patients (85%), with a mean follow-up duration of 76.6 months (range 2–393 months).

Sixty-eight tumours (56.7%) were composed only of MX components, while four tumours (3.3%) contained less than 5% RC components. Forty-eight tumours (40%) contained more than 5% RC components, whereas 33 tumours (27.5%) had more than 25% RC components.

Table 2. Clinicopathological features of 120 cases of myxoid/round cell liposarcoma

Age (years)	>40	38 cases
	≤40	82 cases
Sex	Male	61 cases
	Female	59 cases
Anatomical location	Lower extremity	96 cases
	Upper extremity	10 cases
	Head and neck	6 cases
	Trunk	5 cases
	Intraabdominal or retroperitoneal	3 cases
Size	>5 cm	16 cases
	≤5 cm	89 cases
	Unknown	15 cases
Depth	Deep	117 cases
	Superficial	3 cases
Round cell component (%)	<5	72 cases
	≥5 – <25	15 cases
	≥25	33 cases
Mitoses	>5/50 HPF	97 cases
	≤5/50HPF	23 cases
Necrosis	Absent	87 cases
	>50%	25 cases
	≤ 50%	8 cases
Histological grade (FNCLCC)	1	79 cases
	2	35 cases
	3	6 cases
AJCC stage	Ia	16 cases
	Ib	53 cases
	IIa	1 case
	III	34 cases
	IV	1 case
	Unknown	15 cases

Immunohistochemistry

The results of immunohistochemical analysis are summarized in Table 3. Nuclear accumulation of p53 protein was detected in 5/81 MX components examined (6.2%), whereas it was observed in 7/29 RC components (24.1%) (Figure 2A, B). Over-expression of p53 protein was more frequent in RC components than in MX components ($p = 0.01366$; Table 3). MDM2 over-expression was observed in 5/81 MX components (6.2%) and in 4/29 RC components (13.8%). MDM2 over-expression correlated significantly with p53 expression ($p = 0.0082$). For p14 expression, 4/81 MX components (4.9%) showed reduced expression, while 16/29 RC components (55.2%) showed reduced expression (Figure 2C, D). p16 expression was reduced in 4/81 MX components (4.9%), whereas it was reduced in 20/29 RC components (69%). p14 and p16 expressions were significantly reduced in the RC components in comparison with MX components ($p < 0.0001$; Table 3).

Histologically, tumours comprising more than 5% RCs showed significantly more frequent p53 over-expression ($p = 0.009$; Table 3) and reduced p14 and p16 expression ($p < 0.0001$; Table 3), compared with tumours comprising <5% RCs.

MIB-1 LI in 29 RC components (mean, 14.93) was significantly higher than that in 81 MX components (mean, 5.57) ($p < 0.0001$; Table 3, Figure 2E, F). In the tumours containing both MX and RC components, the higher MIB-1 LI of the two components was taken to be the MIB-1 LI of each tumour. In 90 tumours, the MIB-1 LI was in the range 0.76–49.6 (mean, 8.44). Tumours with ≥5% RCs showed a significantly higher MIB-1 LI (mean, 12.68), compared with that seen in the tumours with <5% RCs (mean, 5.42) ($p < 0.0001$; Table 3). A higher MIB-1 LI correlated significantly with immunohistochemical p53 expression ($p < 0.001$), MDM2 over-expression ($p = 0.0016$), reduced p14 expression ($p < 0.0001$)

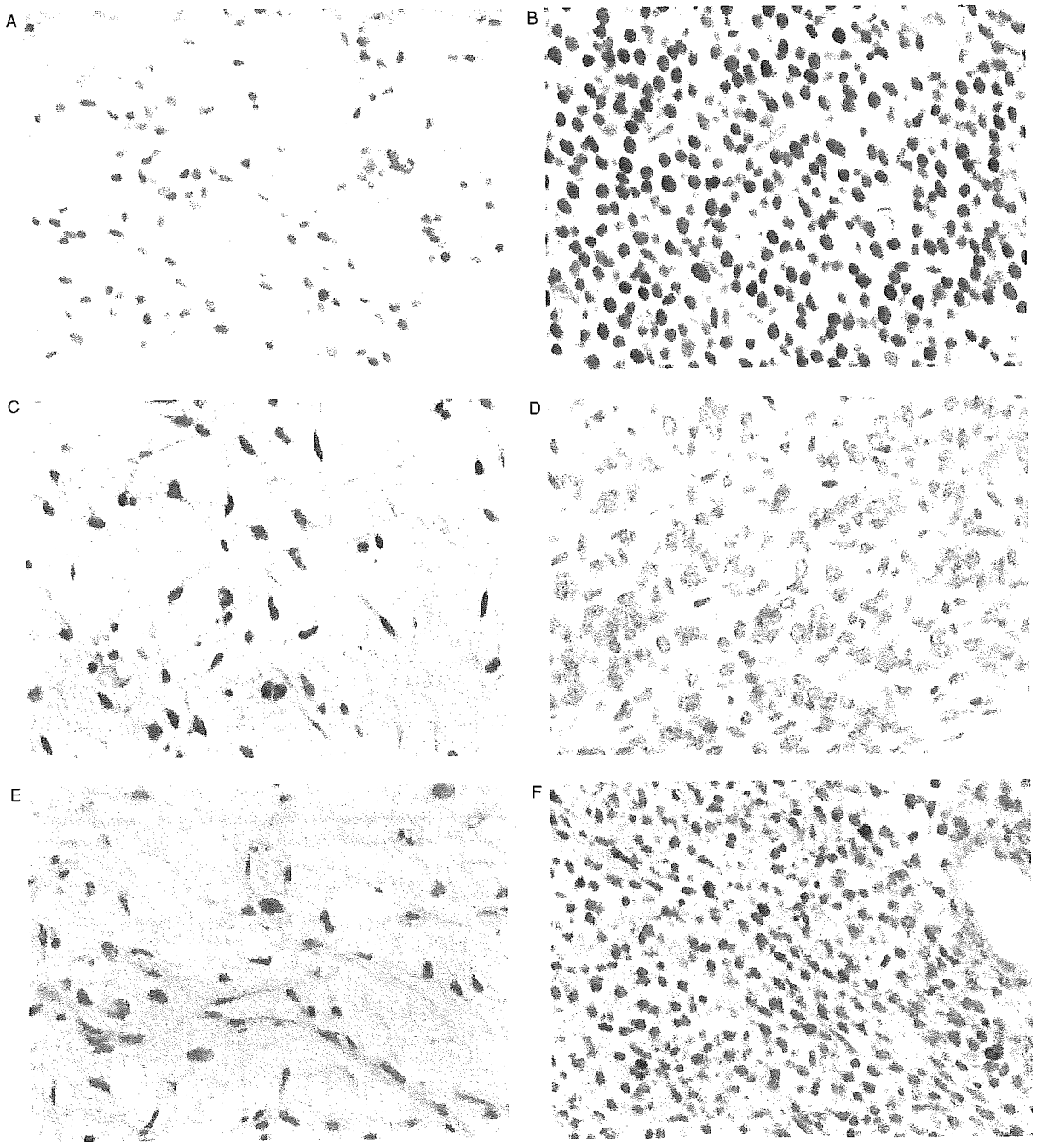

Figure 2. (A, B) p53 immunoreactivity can be seen in both myxoid (A) and round cell (B) components within the same tumour arising in the thigh of a 66 year-old male. (C, D) p14 expression is preserved in the myxoid component (C), whereas it is reduced in the round cell component (D) within the same tumour arising in the knee of a 53 year-old female. (E, F) Myxoid component showing a low MIB-1 LI of 3.3 (E), while the round cell component within the same tumour shows a high MIB-1 LI of 9.2 (F). This patient died of disease 22 months after initial surgery

and reduced p16 expression ($p < 0.0001$) in the 110 components examined (Table 4).

Mutational analysis of the $p16^{INK4a}/p14^{ARF}$ and *p53* genes

The results of mutational analysis of the $p16^{INK4a}/p14^{ARF}$ gene are summarized in Table 5. $p16^{INK4a}/p14^{ARF}$ gene mutational analysis (exon 1α, 2 and 3) was available in 70 samples that included 17 RC components and 53 MX components. Ten mutations (14.3%) in nine cases were detected (Figure 3). Four mutations were present in the RC components, while six mutations were present in the MX components. Eight were missense mutations, whereas the remaining two were silent mutations (Table 5).

Mutation of $p14^{ARF}$ exon 1β was detected in eight samples (12.3%) from eight cases among 65 evaluable samples (18 samples from RC components and 47 samples from MX components). Four mutations were observed in RC components and four mutations were observed in MX components. Four mutations were missense mutations, three were silent mutations, while the remaining mutation was a stop codon (Table 5).

Table 3. Immunohistochemical and molecular genetic comparison between myxoid and round cell component, and in histologic type

	Component				Histologic type			
	Number	MX	RC	*p* Value	Number	RC < 5%	RC ≥ 5%	*p* Value
Immunohistochemical								
p53	+($n = 8$)	5	7	0.01366*	+($n = 8$)	1	7	0.009*
	−($n = 82$)	76	22		−($n = 82$)	51	31	
MDM2	+($n = 9$)	5	4	0.947	+($n = 7$)	3	4	0.3283
	−($n = 101$)	76	25		−($n = 83$)	49	34	
p14	Reduced ($n = 20$)	4	16	<0.0001*	Reduced ($n = 18$)	1	17	<0.0001*
	Preserved ($n = 90$)	77	13		Preserved ($n = 72$)	51	21	
p16	Reduced ($n = 24$)	4	20	<0.0001*	Reduced ($n = 22$)	2	20	<0.0001*
	Preserved ($n = 86$)	77	9		Preserved ($n = 68$)	50	18	
MIB-1 LI	(mean)	5.57	14.931	<0.0001*	(mean)	5.424	12.677	<0.0001*
	(SD)	4.51	9.106		(SD)	4.942	9.198	
Molecular genetic								
p53 mutation	+($n = 8$)	4	4	0.0974	+($n = 8$)	3	5	0.1438
	−($n = 69$)	54	15		−($n = 56$)	36	20	
p53 missense	+($n = 4$)	2	2	0.253	+($n = 4$)	1	3	0.1611
mutation	−($n = 73$)	56	17		−($n = 60$)	38	22	
MDM2	+($n = 8$)	4	4	0.0815	+($n = 7$)	3	4	0.343
amplification	−($n = 51$)	41	10		−($n = 44$)	26	18	
p14 methylation	+($n = 8$)	4	4	0.091	+($n = 8$)	2	6	0.0047*
	−($n = 62$)	49	13		−($n = 52$)	41	11	
p14 HD	+($n = 4$)	3	1	0.7291	+($n = 4$)	3	1	0.398
	−($n = 66$)	49	17		−($n = 57$)	31	26	
p14 mutation	+($n = 14$)	9	5	0.8711	+($n = 13$)	6	7	0.1888
(incl. *p16* exon2)	−($n = 52$)	39	13		−($n = 40$)	26	14	
p16 HD	+($n = 6$)	4	2	0.795	+($n = 6$)	3	3	0.511
	−($n = 48$)	35	13		−($n = 41$)	24	17	
p16 mutation	+($n = 10$)	6	4	0.9448	+($n = 9$)	4	5	0.305
	−($n = 60$)	47	13		−($n = 50$)	30	20	

MX, myxoid component; RC, round cell component; SD, standard deviation; HD, homozygous deletion.
* Statistically significant.

Eight of the 77 evaluable samples (10.4%) from 19 RC components and 58 MX components had *p53* point mutations (Table 6). There were nine mutational sites, five being missense mutations, three silent mutations and one a stop codon (Table 6).

Differential PCR assay for the homozygous deletion of $p16^{INK4a}/p14^{ARF}$ genes and *MDM2* gene amplification

Homozygous deletion (HD) of the $p16^{INK4a}$ gene was detected in 6/54 evaluable samples (11.1%) from 15 RC components and 39 MX components (Figure 4, Table 5). Three HDs were present in the RC components, while the remaining three were in the MX components. Four of 70 evaluable samples (5.7%) from 18 RC components and 52 MX components had $p14^{ARF}$ HD (Figure 4, Table 5). One HD was observed in the RC component and three HDs were present in MX components.

MDM2 gene amplification was detected in 8/59 evaluable samples (13.6%) from 14 RC components and 45 MX components.

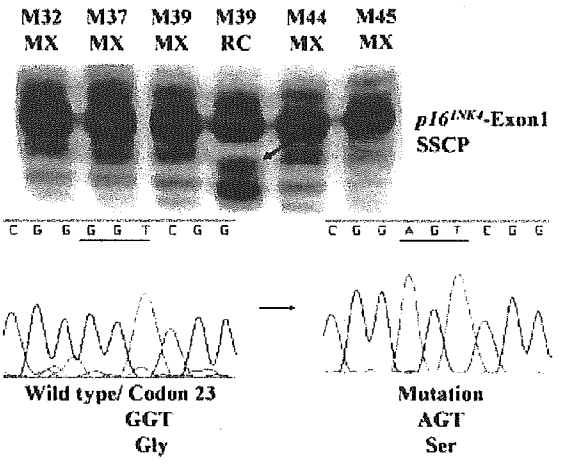

Figure 3. PCR-SSCP and direct DNA sequencing of exon 1α of the $p16^{INK4}$ gene. An abnormally shifted band can be detected in the round cell component (RC) of case M39 (arrow), whereas no abnormalities are observed in the myxoid component (MX) of the same case (M39). There is a G → A transition in codon 23

Methylation-specific PCR for the promoter region of the $p16^{INK4a}/p14^{ARF}$ genes

None of the 52 evaluable samples harboured hypermethylation of the $p16^{INK4a}$ gene (Figure 5). Eight of 70

Table 4. Correlation between immunohistochemical expression of p53, MDM2, p14 and p16 and MIB-1 LI in the 110 components examined

Protein expression		Mean	SD	*p* Value
p53	+($n = 12$)	16.599	12.650	<0.0001*
	−($n = 98$)	7.005	5.637	
MDM2	+($n = 9$)	15.341	15.483	0.0016*
	−($n = 101$)	7.406	5.822	
P14	Reduced ($n = 20$)	14.686	10.148	<0.0001*
	Preserved ($n = 90$)	6.572	5.602	
P16	Reduced ($n = 24$)	14.027	9.981	<0.0001*
	Preserved ($n = 86$)	6.376	5.353	

SD, standard deviation. * Statistically significant.

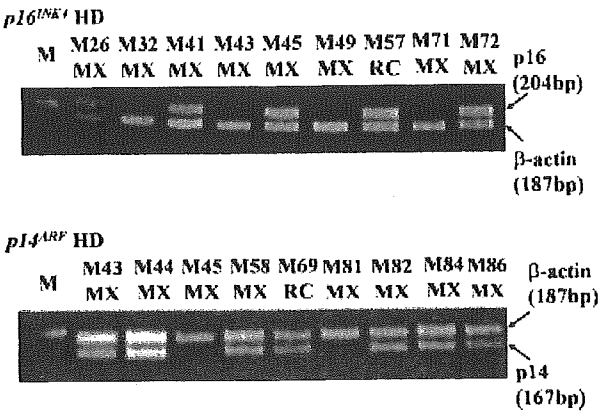

Figure 4. Differential PCR for exons 1α and 1β of the $p16^{INK4}/p14^{ARF}$ homozygous deletion. Myxoid components (MX) of cases M32, M43, M49 and M71 display an absence of the PCR products for the $p16^{INK4}$ gene, while MX of cases M45 and M81 show a lack of PCR products for the $p14^{ARF}$ gene

evaluable samples (11.4%) from 17 RC components and 53 MX components showed hypermethylation within the promoter region of the $p14^{ARF}$ gene (Figure 5, Table 5). Tumours with ≥ 5% RCs showed a significantly higher rate of $p14^{ARF}$ gene hypermethylation (6/17, 35.3%) in comparison with those with less than 5% RCs (2/43, 4.7%) ($p = 0.0047$; Table 3).

Correlation between immunohistochemical results and gene alterations

Although no significant correlation was observed between p53 expression and *p53* mutation status (Table 7), MDM2 over-expression correlated significantly with *MDM2* gene amplification ($p < 0.0001$; Table 7). There was a significant correlation between the reduced expression of p14 protein and hypermethylation of the $p14^{ARF}$ gene ($p = 0.0176$; Table 7). Within the p14 and p53 pathway, immunohistochemically reduced expression of p14 correlated with p53 expression ($p = 0.00837$). However, no correlation was observed between p53 expression and $p14^{ARF}$ gene alteration.

Concerning the correlation between gene alterations and MIB-1 LI, higher MIB-1 LIs showed a significant correlation with *MDM2* over-expression ($p = 0.017$), *p14* mutation ($p = 0.0042$) and *p16* missense mutation ($p = 0.0108$).

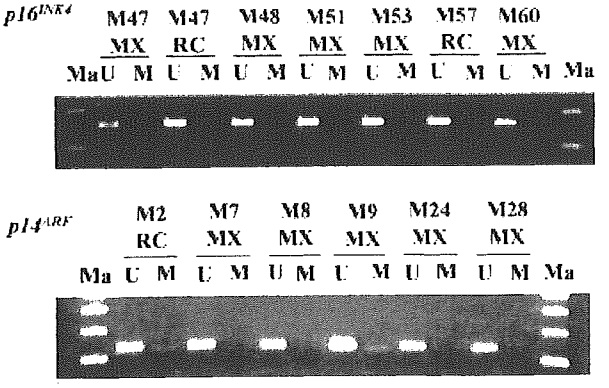

Figure 5. Methylation-specific PCR analysis of the $p16^{INK4}/p14^{AR}$ gene. PCR products amplified using primers specific for unmethylated (U) and methylated (M) DNA. Although no hypermethylation of the $p16^{INK4}$ gene promoter can be observed, the round cell component (RC) of case M2 and the myxoid component (MX) of case M9 show both methylated and unmethylated signals for the $p14^{AR}$ gene promoter

Prognostic factors

The results of survival analysis are summarized in Table 8. Clinicopathologically, age >40 years ($p = 0.0165$), location other than the extremities or trunk ($p < 0.0001$), the presence of an RC component (≥5%, $p = 0.0485$; ≥25%, $p = 0.039$; Figure 6A), the presence of tumour necrosis ($p = 0.0474$), high FNCLCC histological grade (grade 2 or 3; $p = 0.0177$) and high AJCC stage (stage III or IV; $p = 0.0369$) were adverse prognostic factors. Those patients with reduced expression of p14 protein had worse survival than those with preserved p14 expression ($p = 0.0338$; Figure 6B). A high MIB-1 LI of more than 8.4 (mean value) correlated significantly with poor survival ($p < 0.0001$; Figure 6C). Those patients with *p53* mutation ($p = 0.0328$) or *p53* missense mutation ($p = 0.0111$; Figure 6D) had a worse survival than those with no *p53* mutation. Furthermore, multivariate analysis using the Cox model revealed that tumour location ($p = 0.0251$), the presence of more than 25% RC components ($p = 0.0113$), a high histological grade ($p = 0.0318$), a high AJCC stage ($p = 0.0318$), a high MIB-1 LI of >8.4 ($p = 0.0005$) and *p53* missense mutation ($p = 0.0036$) were independent and significant factors for poor prognosis.

Discussion

Round cell (RC) components are identified in about 50% of MLS/RCLSs and have been shown to be a powerful predictor of poor prognosis [5–8,10]. In our large, extensively sampled series, 48/120 cases (40%) contained >5% RC components. Some authors [6,9] have reported that 5% RC components is a prognostic factor, while others [7,8,11] have demonstrated 25% as the cut-off point. In the current study, the presence of

Table 5. $p16^{INK4a}$ and $p14^{ARF}$ alterations in myxoid/round cell liposarcoma

				$p16^{INK4a}$				$p14^{ARF}$				
Number	**Age/sex**	**Location**	**Type**	**ME**	**HD**	**Mutation**	**IHC**	**ME**	**HD**	**Exon 1-β mutation**	**IHC**	**Prognosis**
M32-RC	49/F	Thigh	M/R	NA	(+)	NA	(−)	NA	(−)	Codon 40 GGC(Gly) ≫ GGA(Gly)	(+)	58M DOD
M43-RC	77/F	Retroperitoneum	M/R	NA	(+)	NA	(−)	(−)	(−)	(−)	(−)	9M DOD
M43-MX				(−)	(−)	(−)	(−)	(+)	(−)	(−)	(−)	
M49-MX	29/F	Thigh	M	NA	(+)	NA	(+)	(−)	(−)	(−)	(+)	NA
M104-MX	54/F	Buttock	M	NA	(+)	NA	(+)	(−)	(−)	(−)	(+)	105M NED
M91-MX	47/F	Thigh	M	NA	(+)	NA	(+)	NA	(−)	Codon 57 CIAO(Gly) ≫ AAG(Lys)	(+)	18M DOD
M71-MX	66/M	Thigh	M/R	NA	(+)	NA	(+)	(−)	(−)	(−)	(+)	55M NED
M58-RC	66/F	Retroperitoneum	M/R	NA	NA	Codon 28 GTG(Val) ≫ ATG(Met)	(+)	(−)	(−)	(−)	(+)	14M AWD
M39-RC	28/M	Thigh	M/R	NA	NA	Codon 23 GGT(Gly) ≫ AGT(Ser)	(−)	(+)	(−)	(−)	(−)	22M DOD
M105-RC	29/M	Upper arm	M/R	(−)	(−)	Codon 15 TGG(Trp) ≫ CAG(Gln)	NA	NA	(−)	(−)	(+)	NA
M36-MX	44/M	Abdominal cavity	M	(−)	NA	Codon 134 GCG(Ala) ≫ ACG(Thr)*	(+)	(−)	(−)	(−)	(+)	46M DOD
M25-MX	51/M	Thigh	M	NA	NA	Codon 134 GCG(Ala) ≫ ACG(Thr)*	(+)	NA	(+)	NA	(+)	139M DOD
M50-MX	67/M	Popliteal fossa	M	NA	NA	Codon 131 CGC(Arg) ≫ CAC(His)*	(+)	NA	NA	NA	(+)	108M NED
M47-MX	40/M	Thigh	M/R	(−)	(−)	Codon 68 GCG(Ala) ≫ ACG(Thr)*	(+)	(−)	(−)	(−)	(−)	38M NED
M47-RC				(−)	(−)	Codon 68 GCG(Ala) ≫ ACG(Thr)*	(−)	(−)	(−)	(−)	(−)	
M19-MX	30/F	Thigh	M	(−)	(−)	Codon 27 GAG(Glu) ≫ GAA(Glu)	(+)	(−)	(−)	(−)	(+)	249M NED
M72-MX	35/M	Thigh	M	(−)	(−)	Codon 115 GTG(Val) ≫ GTA(Val)*	(+)	(−)	(−)	(−)	(−)	51M NED
M26-RC	31/M	Shoulder	M/R	(−)	(−)	NA	(−)	(+)	(−)	NA	(−)	130M NED
M2-RC	43/M	Lower leg	M/R	(−)	(−)	(−)	(−)	(+)	(−)	(−)	(−)	22M AWD
M53-MX	56/F	Thigh	M	(−)	(−)	(−)	(+)	(+)	(−)	(−)	(+)	98M NED
M106-RC	44/M	Thigh	M/R	(−)	(−)	(−)	(+)	(+)	(−)	(−)	(−)	103M DOD
M63-MX	28/F	Thigh	M	(−)	(−)	(−)	(+)	(+)	(−)	(−)	(+)	111M NED
M9-MX	30/M	Abdominal wall	M/R	(−)	(−)	(−)	(+)	(+)	(−)	(−)	(+)	NA
M81-RC	44/M	Knee	M/R	NA	NA	(−)	(−)	NA	(+)	NA	(−)	27M NED
M30-MX	18/M	Cheek	M	NA	NA	NA	(+)	NA	(+)	NA	(+)	48M DOD
M45-MX	63/F	Thigh	M	(−)	(−)	(−)	(+)	NA	(+)	NA	(+)	31M DOD
M8-RC	53/F	Knee	M/R	(−)	(−)	(−)	(−)	(−)	(−)	Codon 42 CCG(Pro) ≫ CTG(Leu)	(+)	4M AWD
M64-MX	54/M	Retroperitoneum	M	(−)	(−)	(−)	(+)	(−)	(−)	Codon 85 CCT(Pro) ≫ TCT(Ser)	(+)	9M DOD
M35-MX	33/F	Lower leg	M	NA	NA	(−)	(+)	NA	(−)	Codon 80 GGG(Gly) ≫ GAG(Glu)	(+)	NA
M18-RC	27/F	Retroperitoneum	M/R	NA	NA	NA	(−)	NA	NA	Codon 82 CAG(Gln) ≫ TAG(stop)	(−)	NA
M80-MX	38/M	Thigh	M/R	(−)	(−)	(−)	(+)	(−)	(−)	Codon 3 TGC(Leu) ≫ TGT(Leu)	(+)	42M DOD
M67-RC	64/F	Chest wall	M/R	NA	NA	NA	(−)	NA	NA	Codon 30 TTG(Leu) ≫ TTA(Leu)	(−)	107M NED

MX, mysoil component; RC, round cell component; M/R, tumour with more than 5% of round cells; M tumour with less than 5% of round cells; NA, data not available; DOD died of disease; NED, no evidence of diseases; AWD, alive with disease; ME, methylation; HD, homozygous deletion, IHC, immunohistochemistry. Share with $p14^{ARF}$ gene mutation (exon2).